# Chapter 2
# Solitary Quantum Dot Laser

## 2.1 Introduction

In this chapter, the model for the solitary semiconductor QD laser is introduced and its turn-on dynamics is studied. As already discussed in the introduction, one striking difference distinguishing QD from conventional semiconductor QW lasers is their special carrier scattering dynamics between the discrete QD levels and the continuous sub-bands of the surrounding carrier reservoir [1, 2]. For instance, this scattering dynamics is responsible for the strongly damped ROs of QD lasers in comparison to QW lasers [3–7].

Our modeling approach aims to study in detail the dependence of the dynamics of the QD laser on the carrier scattering dynamics. Therefore, a microscopically based rate equation model is introduced that assumes a classical light field, but takes into account microscopically calculated Coulomb scattering rates for the carrier exchange between QD and carrier reservoir as discussed in [5, 8–11] (see [12] for a concise review). The microscopically calculated Coulomb scattering rates yield nonlinear carrier lifetimes $\tau_e$ and $\tau_h$ for electrons and holes in the QD levels, which strongly depend on the band structure, i.e., on the size and the material composition of the QDs, as well as on the filling of the carrier reservoir and thus on the pump current [5, 13]. Further, in this microscopic modeling approach it is taken into account that the energetic distances of the QD levels and the band edges of the carrier reservoir are different for electrons and holes, which results in different dynamics for electrons and holes in the QD levels as well as in the carrier reservoir. Therefore, in a hierarchy of semiconductor modeling approaches (see [14] for an overview), the model bridges the gap between simple rate equation models and full quantum-mechanic modeling approaches, which treat also the light field quantum-mechanically and permit to study the photon statistic of the emitted light [15, 16]. Simpler rate equation models take into account only one carrier type, i.e., the dynamics of electron-hole pairs is modeled. Further, the carrier exchange between QDs and carrier reservoir is, in these models, described by constant carrier lifetimes in the QD levels [17], or by linear in-scattering rates and constant out-scattering rates [18, 19].

C. Otto, *Dynamics of Quantum Dot Lasers*,
Springer Theses, DOI: 10.1007/978-3-319-03786-8_2,

Our model is kept simple enough to derive analytical expression for RO frequency and damping. Therefore, a variety of effects has been neglected. For instance, a more complex modeling approach has to be chosen if changes in the emission wavelength due to Coulomb enhancement are of interest [20–25]. Furthermore, to study ultrafast coherent dynamics on the fs-scale, for example, the gain recovery in QD-based optical amplifiers [26], the dynamics of the microscopic polarization becomes important, which has been eliminated adiabatically in our model. To model the dynamics of the microscopic polarization, semiconductor Bloch equations have to be considered [27–31].

This chapter is organized as follows. After an introduction to the QD laser model in Sect. 2.2, the dynamical equations are non-dimensionalized in Sect. 2.3. Then, the turn-on dynamics of the QD laser is studied for different band structures in Sect. 2.4, and in Sect. 2.5, analytical expressions for the steady states as well as RO frequency and damping of the QD laser are presented for different band structures. These expressions reveal how the damping of the ROs is increased with respect to QW lasers by the carrier lifetimes $\tau_e$ and $\tau_h$. Finally, a summary is given in Sect. 2.6.

## 2.2 Quantum Dot Laser Model

In this section, the dynamical equations modeling the solitary QD laser are introduced. The QDs are embedded into a two dimensional QW acting as a carrier reservoir. A band structure of the device is depicted in Fig. 2.1. The crucial parameters are the confinement energies $\Delta E_e$ and $\Delta E_h$ that mark the energy differences between the QD ground state and the band edge of the surrounding QW for electrons and holes, respectively. The QD laser model is based on the model described in [5, 13], which has shown good quantitative agreement with experiments regarding the turn-on behavior and the modulation response of QD lasers [13]. The nonlinear, coupled, and five-variable rate equation model including the photon number in the cavity $N_{\mathrm{ph}}$, as well as the electron and hole occupation probabilities in the QDs, $\rho_e$ and $\rho_h$, and the electron and hole densities in the QW, $w_e$ and $w_h$, respectively, is given by the following equations

$$\frac{dN_{\mathrm{ph}}}{dt} = \left[2\bar{W}Z_a^{QD}(\rho_e+\rho_h-1)-2\kappa\right]N_{\mathrm{ph}}+\beta 2Z_a^{\mathrm{QD}}W\rho_e\rho_h, \tag{2.1a}$$

$$\frac{d\rho_e}{dt} = S_e^{\mathrm{in}}(1-\rho_e)-S_e^{\mathrm{out}}\rho_e-\bar{W}(\rho_e+\rho_h-1)N_{\mathrm{ph}}-W\rho_e\rho_h, \tag{2.1b}$$

$$\frac{d\rho_h}{dt} = S_h^{\mathrm{in}}(1-\rho_h)-S_h^{\mathrm{out}}\rho_h-\bar{W}(\rho_e+\rho_h-1)N_{\mathrm{ph}}-W\rho_e\rho_h, \tag{2.1c}$$

$$\frac{dw_e}{dt} = \frac{j}{e_0}-2N^{\mathrm{QD}}\left[S_e^{\mathrm{in}}(1-\rho_e)-S_e^{\mathrm{out}}\rho_e\right]-B^S w_e w_h, \tag{2.1d}$$

$$\frac{dw_h}{dt} = \frac{j}{e_0}-2N^{\mathrm{QD}}\left[S_h^{\mathrm{in}}(1-\rho_h)-S_h^{\mathrm{out}}\rho_h\right]-B^S w_e w_h. \tag{2.1e}$$

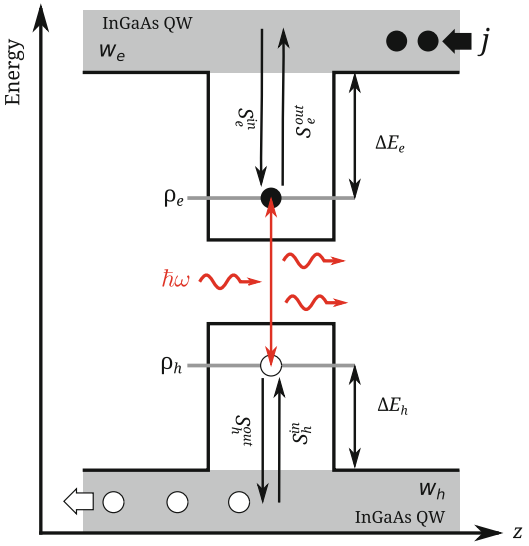


**Fig. 2.1** Energy diagram of the band structure across a QD. The ground state lasing energy is labeled by $\hbar\omega$. The energetic distances of the QD levels from the band edge of the carrier reservoir (QW) for electrons and holes are marked by $\Delta E_e$ and $\Delta E_h$, respectively. The Auger in- and out-scattering rates between QD levels and QW are denoted by $S^{\text{in}}_{e/h}$ and $S^{\text{out}}_{e/h}$, respectively. The occupation probabilities of the QDs are denoted by $\rho_{e/h}$, the reservoir carrier densities are labeled by $w_{e/h}$, and $j$ is the pump current density

Here, $2\kappa$ are the optical intensity losses, which are balanced by the linear gain term $2\bar{W}Z_a^{\text{QD}}(\rho_e+\rho_h-1)$, where $\bar{W}Z_a^{\text{QD}}$ is the linear gain coefficient for the processes of induced emission and absorption. The gain coefficient is proportional first to the Einstein coefficient of induced emission $\bar{W}$ that measures the coherent interaction between the two-level system and the laser mode, and second to the number $Z_a^{\text{QD}}$ of lasing QDs inside the waveguide (the factor 2 is due to spin degeneracy). A detailed derivation of $\bar{W}$ may be found in [32, 33]. The number of lasing QDs, $Z_a^{\text{QD}}$, is given by $Z_a^{\text{QD}} \equiv a_L A N_a^{\text{QD}}$, where $a_L$ is the number of self-organized QD layers, $A$ is the in-plane area of the QW, and $N_a^{\text{QD}}$ is the density per unit area of the active QDs. As a result of the size distribution and of the material composition fluctuations of the QDs, the gain spectrum is inhomogeneously broadened, and only a subgroup (density $N_a^{\text{QD}}$) of all QDs ($N^{\text{QD}}$) matches the mode energies for lasing. The spontaneous emission from one QD is taken into account by the term $W\rho_e\rho_h$, where $W$ is the Einstein coefficient for spontaneous emission. It can be determined by calculating the coherent interaction of a two-level system, i.e., a single QD, with all resonator modes in the framework of the second quantization [14]. Note that the coefficients $\bar{W}$ and $W$ differ by three orders of magnitude. The spontaneous emission factor measuring the probability that a spontaneously emitted photon is emitted into the lasing mode is denoted by $\beta$. The spontaneous emission in the QW is incorporated by $B^S w_e w_h$, where $B^S$ is the band-band recombination coefficient. The carriers are first injected into the carrier reservoir with the current density $j$, and $e_0$ is the elementary charge. In the lasing regime, where the reservoir carrier densities $w_e$ and $w_h$ are very high, Coulomb scattering, i.e., nonlocal Auger recombination, is the dominant carrier exchange process between reservoir and discrete QD levels, and phonon scattering may be neglected [34–37]. This is also supported by the modeling of carrier transport

in QD structures [38, 39]. Nevertheless, phonon scattering is taken into account for the intra-band cooling processes in the reservoir. Thus, for the calculation of the Coulomb scattering rates a quasi-equilibrium within the carrier reservoir is assumed, which is realized by fast phonon intra-band scattering. The Coulomb scattering rates are calculated microscopically within the framework of the Boltzmann equation and an orthogonalized plane-wave approach [8, 9]. The Coulomb interaction is treated in the second-order Born approximation in the Markov limit up to the second order in the screened Coulomb potential [40, 41]. All relevant electron-electron, hole-hole, and mixed processes are included. A detailed discussion of the scattering processes can be found in [28, 42, 43]. The nonlinear scattering rates are denoted by $S_e^{\text{in}}$ and $S_h^{\text{in}}$ for electron and hole capture into the QD levels and by $S_e^{\text{out}}$ and $S_h^{\text{out}}$ for carrier escape to the reservoir, respectively (see Fig. 2.1). The scattering rates depend on the reservoir densities $w_e$ and $w_h$, and are thus pump current dependent.

In thermodynamic equilibrium, there is a detailed balance between in- and out-scattering rates, which allows one to relate the coefficients of in- and out-scattering even away from the thermodynamic equilibrium [44]. The detailed balance relation for in- and out-scattering rates for the quasi-equilibrium then reads [5, 11]

$$S_e^{\text{out}}(w_e, w_h) = S_e^{\text{in}}(w_e, w_h) e^{-\frac{\Delta E_e}{k_{\text{bo}}\mathcal{T}}} \left[ e^{\frac{w_e}{D_e k_{\text{bo}}\mathcal{T}}} - 1 \right]^{-1}, \tag{2.2a}$$

$$S_h^{\text{out}}(w_e, w_h) = S_h^{\text{in}}(w_e, w_h) e^{-\frac{\Delta E_h}{k_{\text{bo}}\mathcal{T}}} \left[ e^{\frac{w_h}{D_h k_{\text{bo}}\mathcal{T}}} - 1 \right]^{-1}. \tag{2.2b}$$

Here, $\Delta E_e \equiv E_e^{\text{QW}} - E_e^{\text{QD}}$ and $\Delta E_h \equiv E_h^{\text{QD}} - E_h^{\text{QW}}$ are the energy differences between the QD levels, $E_e^{QD}$ and $E_h^{\text{QD}}$, and the band edges of the QW, $E_e^{QW}$ and $E_h^{\text{QW}}$, for electrons and holes, respectively. The carrier degeneracy concentrations are given by $D_{e/h} k_{\text{bo}} \mathcal{T}$, where $D_{e/h} \equiv m_{e/h}/(\pi\hbar^2)$ are the 2D densities of state in the carrier reservoir with the effective masses $m_{e/h}$. The temperature is denoted by $\mathcal{T}$ and $k_{\text{bo}}$ is Boltzmann's constant. Figure 2.2a–d depict electron in- and out-scattering rates ($S_e^{\text{in}}$ and $S_e^{\text{out}}$) as well as hole in-and out-scattering rates ($S_h^{\text{in}}$ and $S_h^{\text{out}}$) in terms of the electron density $w_e$ in the carrier reservoir for three fixed ratios $w_h/w_e$ of hole and electron densities. The energy spacings are $\Delta E_e = 210$ meV and $\Delta E_h = 50$ meV for electron and holes, respectively. Crosses mark microscopically calculated values, while colored lines depict the fit functions given in Appendix A.0.1. Gray dashed and black dash-dotted vertical lines denote the steady state values of $w_e$ close to ($j = 1.5\, j_{\text{th}}$) and well above threshold ($j = 3.5\, j_{\text{th}}$), where $j_{\text{th}}$ denotes the threshold current density. $j_{\text{th}}$ is the current density, at which the induced emission starts to dominate the induced absorption and the cavity losses [45].

Hole in- and out-scattering rates are larger than their electronic counterparts, due to the smaller energetic distances of the QD level of the holes to the band edge of the reservoir. For low reservoir densities, the in-scattering rates increase quadratically with $w_e$ as expected from mass action kinetics.

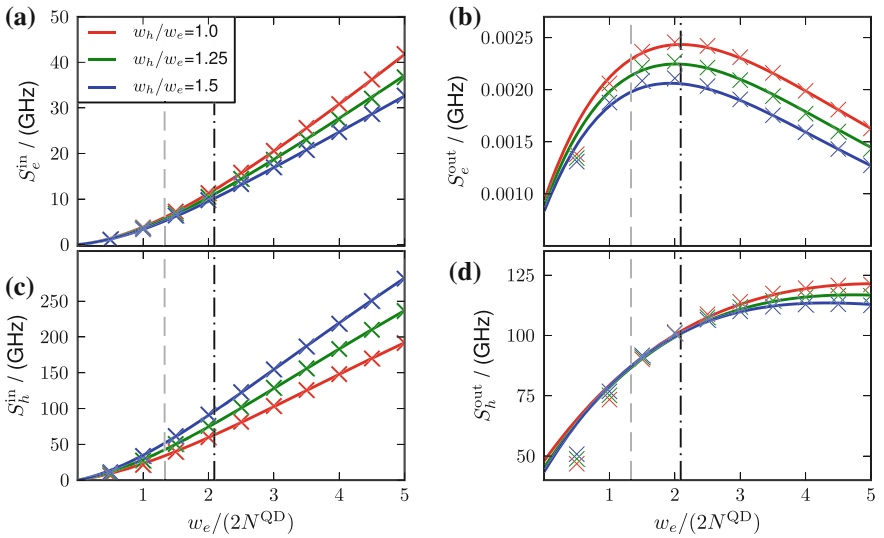


**Fig. 2.2** In- and out-scattering rates for electrons ($S_e^{\mathrm{in}}$ (**a**) and $S_e^{\mathrm{out}}$ (**b**)) and holes ($S_h^{\mathrm{in}}$ (**c**) and $S_h^{\mathrm{out}}$ (**d**)), respectively, in dependence of the electron density in the carrier reservoir $w_e$ (normalized to $2N^{\mathrm{QD}}$). The energy spacings between the band edges of the carrier reservoir and the discrete energy levels of the QDs are $\Delta E_e = 210$ meV and $\Delta E_h = 50$ meV for electrons and holes, respectively (reference rates). Crosses denote results of microscopic calculations and lines denote fit functions given in Appendix A.1. *The gray dashed* and *the dash-dotted black lines* denote steady state values of $w_e$ for pump current densities of $j = 1.5\,j_{\mathrm{th}}$ and $j = 3.5\,j_{\mathrm{th}}$, respectively, and $j_{\mathrm{th}}$ is the current density at lasing threshold. Different colors denote different ratios $w_h/w_e$ of hole ($w_h$) and electron ($w_e$) densities in the carrier reservoir. Parameters as in Table 2.2

The carrier lifetimes $\tau_e$ and $\tau_h$ that result from Coulomb scattering between QDs and carrier reservoir are defined by the nonlinear scattering rates as

$$\tau_e \equiv (S_e^{\mathrm{in}} + S_e^{\mathrm{out}})^{-1} \quad \text{and} \quad \tau_h \equiv (S_h^{\mathrm{in}} + S_h^{\mathrm{out}})^{-1}. \tag{2.3}$$

It is important to note that these lifetimes are not constant but depend on the carrier densities in the surrounding carrier reservoir and thus on the injected pump current. They constitute the additional time scales that distinguishes QD from QW lasers. In the following chapters, their importance for the turn-on dynamics of the laser as well as for its dynamical response to external optical injection and feedback will be discussed. One advantage of QD lasers is that the additional lifetimes $\tau_e$ and $\tau_h$ can be tuned by the growth conditions and the material composition of the QDs [1], which changes the energy spacings $\Delta E_e$ and $\Delta E_h$ between the band edge of the carrier reservoir and the QD levels. The energy spacings determine how $\tau_e$ and $\tau_h$ compare to the carrier lifetimes in the carrier reservoir and the photon lifetime. The pump dependent steady state values of $\tau_e$ and $\tau_h$ are shown in Fig. 2.3 for three different QD structures, which are compared throughout this work. The different structures

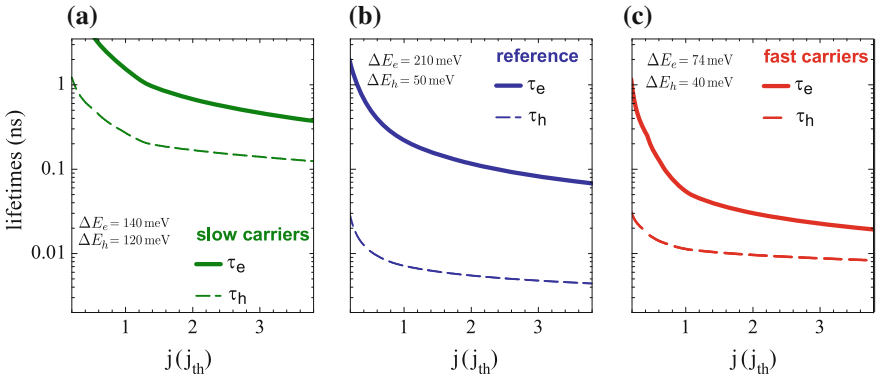


**Fig. 2.3** Nonlinear steady state carrier lifetimes $\tau_e$ and $\tau_h$ for electrons and holes, respectively, as resulting from the microscopically calculated scattering rates calculated microscopically for (**a**) slow, (**b**) reference, and (**c**) fast rates (see Table 2.1). Parameters as in Table 2.2. Modified from [32]

**Table 2.1** Energy differences $\Delta E_e$ and $\Delta E_h$ between carrier reservoir and QD ground state for the three different sets of scattering rates used for the simulations as well as steady state carrier lifetimes for electrons ($\tau_e$) and holes ($\tau_h$)

| Data set | $\Delta E_e$ (meV) | $\Delta E_h$ (meV) | $\tau_e$ (ns) | $\tau_h$ (ns) |
|---|---|---|---|---|
| Slow | 140 | 120 | 0.395 | 0.129 |
| Reference | 210 | 50 | 0.071 | 0.005 |
| Fast | 74 | 40 | 0.021 | 0.01 |

For a pump current density of $j = 3.5 j_{\text{th}}$ ($j_{\text{th}}$ is the pump current density at lasing threshold.)

are modeled by using three different sets of confinement energies between QD and carrier reservoir listed in Table 2.1.

By controlling the growth mode during epitaxy, it is possible to create QDs with different size and composition. As such the reference rates plotted in Fig. 2.3b result from QDs with a base length of $18 \times 18$ nm and a ratio of 10 between the effective masses of holes and electrons (as used in [13]). They are named "reference", because with these rates, good agreement of the QD model with experimental turn-on curves is observed [5]. Figure 2.4 shows the turn-on dynamics of the photon number $N_{\text{ph}}$ as measured from experiment (black stars), which is superimposed by the calculated turn-on dynamics for $j = 2.2 j_{\text{th}}$ and $j = 2.7 j_{\text{th}}$ (blue lines), respectively. Typical for QD lasers is the strong suppression of the ROs.

Differences in the effective masses (e.g. obtained by changing the QD composition) are expressed in a different ratio between electron and hole confinement energy (see [11]). Figure 2.3a depicts the case of large confinement energies that are similar for electrons and holes, i.e., $\Delta E_e \approx \Delta E_h$, resulting in long Auger scattering lifetimes. Increasing the size of the dots leads to smaller confinement energies (shallow dots with smaller energetic distance between the QD levels and carrier reservoir) and thus to the fast scattering rates (Fig. 2.3c). Fit function for the three sets of scattering

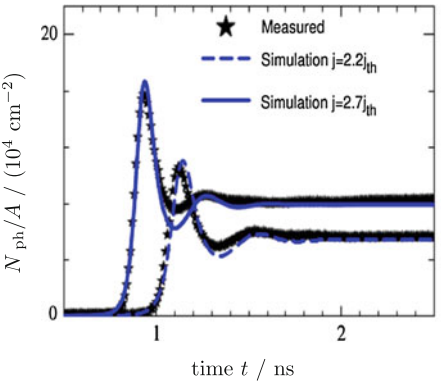


**Fig. 2.4** QD laser turn-on after the pump current $j_{\text{th}}$ is switched on simulated with the reference rates (*blue curves*) and compared to experimental results (*black stars*) for $j = 2.2\,j_{\text{th}}$ and $j = 2.7\,j_{\text{th}}$, respectively. Modified from [10]

**Table 2.2** Physical parameters used in the simulation of the QD laser model unless stated otherwise

| Symbol | Value | Symbol | Value | Symbol | Value |
|---|---|---|---|---|---|
| $W$ | $0.7\ \text{ns}^{-1}$ | $A$ | $4 \times 10^{-5}\,\text{cm}^2$ | $\mathcal{T}$ | 300 K |
| $\bar{W}$ | $0.11\,\mu\text{s}^{-1}$ | $N_a^{\text{QD}}$ | $0.3 \times 10^{10}\,\text{cm}^{-2}$ | $L$ | 1 mm |
| $2\kappa$ | $0.1\ \text{ps}^{-1}$ | $N^{\text{QD}}$ | $1 \times 10^{11}\,\text{cm}^{-2}$ | $\varepsilon_{bg}$ | 14.2 |
| $\beta$ | $2.2 \times 10^{-3}$ | $B^S$ | $540\ \text{ns}^{-1}\,\text{nm}^2$ | $\tau_{\text{in}}$ | 24 ps |
| $a_L$ | 15 | $Z_a^{QD}$ | $1.8 \times 10^6$ | $m_e$ | $0.043\,m_0$ |
| $\lambda_{\text{opt}}$ | 1.3 µm | $\nu_{las}$ | 230 THz | $m_h$ | $0.45\,m_0$ |

rates can be found in the Appendix A. All other numerical parameters that were used in the simulation are shown in Table 2.2.

## 2.3 Non-dimensionalized Rate Equations

For the subsequent study of the dynamical equations (2.1), they are rewritten into a dimensionless form. This has two advantages: on the one hand, the number of independent parameters is reduced by combining them into dimensionless groups, which can be for example time scale ratios. On the other hand, dimensionless equations are better suited for numerical simulations, because very large and very small numbers are avoided [46, 47]. As it is usually done for rate equation models of semiconductor lasers, time is rescaled with respect to the photon lifetime $\tau_{\text{ph}} \equiv (2\kappa)^{-1}$ [48] by introducing the dimensionless time $t' \equiv 2\kappa t$. Furthermore, dimensionless reservoir populations $W_e \equiv w_e/(2N^{\text{QD}})$ and $W_h \equiv w_h/(2N^{\text{QD}})$ are introduced, which are of order one. The dynamical equations (2.1) then read

$$N'_{\mathrm{ph}} = \rho_{\mathrm{inv}}(\rho_e, \rho_h) N_{\mathrm{ph}} + d\rho_e\rho_h, \tag{2.4a}$$

$$\rho'_e = \gamma\Big[F_e(\rho_e, \rho_h, W_e, W_h) - r_w(\rho_e + \rho_h - 1)N_{\mathrm{ph}} - \rho_e\rho_h\Big], \tag{2.4b}$$

$$\rho'_h = \gamma\Big[F_h(\rho_e, \rho_h, W_e, W_h) - r_w(\rho_e + \rho_h - 1)N_{\mathrm{ph}} - \rho_e\rho_h\Big], \tag{2.4c}$$

$$W'_e = \gamma\Big[J - F_e(\rho_e, \rho_h, W_e, W_h) - cW_eW_h\Big], \tag{2.4d}$$

$$W'_h = \gamma\Big[J - F_h(\rho_e, \rho_h, W_e, W_h) - cW_eW_h\Big], \tag{2.4e}$$

where $(\cdot)'$ denotes differentiation with respect to the dimensionless time $t'$. In Eq. (2.4a) a rescaled inversion $\rho_{\mathrm{inv}}$ was introduced, which is defined as[1]

$$\rho_{\mathrm{inv}}(\rho_e, \rho_h) \equiv \frac{1}{2}\left[g(\rho_e + \rho_h - 1) - 1\right]. \tag{2.5}$$

Since the occupation probabilities $\rho_e$ and $\rho_h$ are restricted to values between zero and one, $\rho_{\mathrm{inv}}$ is in turn restricted to

$$-\frac{(g+1)}{2} \leq \rho_{\mathrm{inv}} \leq \frac{g-1}{2}.$$

The functions $F_e$ and $F_h$ contain the contributions of the scattering rates

$$F_e(\rho_e, \rho_h, W_e, W_h) \equiv s_e^{\mathrm{in}}(W_e, W_h)(1 - \rho_e) - s_e^{\mathrm{out}}(W_e, W_h)\rho_e, \tag{2.6a}$$

$$F_h(\rho_e, \rho_h, W_e, W_h) \equiv s_h^{\mathrm{in}}(W_e, W_h)(1 - \rho_h) - s_h^{\mathrm{out}}(W_e, W_h)\rho_h. \tag{2.6b}$$

Here, dimensionless in-scattering rates ($s_e^{\mathrm{in}}, s_e^{\mathrm{out}}$) and out-scattering rates ($s_e^{\mathrm{out}}, s_h^{\mathrm{out}}$), dimensionless carrier lifetimes ($t_e, t_h$), the linear gain coefficient $g$, the ratio of photon and carrier lifetimes $\gamma$, the ratio of the Einstein-factors of induced and spontaneous emission $r_w$, the dimensionless pump rate $J$, the spontaneous emission coefficient $d$, and the coefficient of spontaneous and non-radiative losses in the carrier reservoir $c$ have been introduced as follows

$$s_{e/h}^{\mathrm{in/out}} \equiv \frac{1}{W} S_{e/h}^{\mathrm{in/out}}, \qquad t_{e/h}^{-1} \equiv \frac{1}{W}(S_{e/h}^{\mathrm{in}} + S_{e/h}^{\mathrm{in/out}}), \qquad g \equiv \frac{2a_L \bar{W} A N_a^{\mathrm{QD}}}{2\kappa},$$

$$r_w \equiv \frac{\bar{W}}{W}, \qquad \gamma \equiv \frac{W}{2\kappa}, \qquad J \equiv \frac{j}{e_0 2 N^{\mathrm{QD}} W},$$

[1] For this model, $\rho_{\mathrm{inv}}$ is not a very useful coordinate to simplify the calculation of the steady states, because there is no simple expression for the spontaneous emission terms $-\rho_e\rho_h$ in the QD Eqs. (3.12c) and (3.12d) in terms of $\rho_{\mathrm{inv}}$. However, introducing $\rho_{\mathrm{inv}}$ permits to directly compare the modeling results with most of the literature on three variable models ($R, \Psi, \rho_{\mathrm{inv}}$) of QW lasers under optical injection, where the rescaled inversion is usually denoted by $N$ or $Z$. For recent reviews of the literature see for example [48] and [49].

**Table 2.3** Parameter values for the dimensionless dynamical equations for the QD laser (Eqs. (2.4)) that correspond to the physical parameters given in Table 2.2

| Parameters | Value | Meaning |
|---|---|---|
| $g$ | 3.78 | Linear gain parameter |
| $\gamma$ | $7 \times 10^{-3}$ | Ratio of photon and carrier lifetime |
| $r_w$ | $1.5 \times 10^{-4}$ | Ratio of Einstein-factors of induced and spont. emission |
| $c$ | 1.54 | Spontaneous and non-radiative losses in QW |
| $d$ | 55.44 | Coefficient of spontaneous emission |

$$d \equiv \beta \frac{W Z_a^{\mathrm{QD}}}{\kappa}, \qquad c \equiv \frac{B^S 2 N^{\mathrm{QD}}}{W}. \tag{2.7}$$

The values of the dimensionless parameters $g$, $\gamma$, $c$, and $r_w$, which correspond to the physical parameters of Table 2.2, are listed in Table 2.3.

For the subsequent analysis, it is crucial to note that the carrier equations (2.4b)–(2.4e) are not independent but contain carrier conservation, which can be seen by verifying that

$$\rho_e' + W_e' = \rho_h' + W_h' \tag{2.8}$$

holds. Thus, $\rho_e - \rho_h + W_e - W_h$ is a constant to be determined by the initial conditions. In the absence of doping, this constant is zero and the effect of reservoir doping can be included by choosing a non-zero initial value for one of the reservoir densities, i.e., $n$-doping is described by $W_e \neq 0$ and $p$-doping by $W_h \neq 0$ [11]. Due to the carrier conservation, one dynamical variable can be eliminated by expressing one carrier type in terms of the others, i.e.,

$$W_h = \rho_e + W_e - \rho_h. \tag{2.9}$$

## 2.4 Turn-on Dynamics

In their dimensionless form, the dynamical Eqs. (2.4) directly reveal the different time scales that determine the dynamics. It has been proposed by Tredicce at al. in [50] that lasers may be classified by the ratio of three important time scales given by the decay of the polarization, of the field in the cavity, and of the carriers:

(i) In **class C** lasers, these three dynamical variables decay on the same time scale. This leads to complex dynamics, and chaotic behavior may be observed already for the solitary laser.

(ii) In **class B** lasers, the polarization decays on a much faster time scale (femtoseconds) than the field in the cavity, and may be eliminated adiabatically. Furthermore, a time scale separation exists between the fast photon and the slower carrier subsystem, i.e., the photon lifetime $\tau_{\mathrm{ph}}$ (tenth of picoseconds)

is much smaller than the carrier lifetime $\tau_c$ (nonoseconds). This means that the laser is a slow-fast system and thus responds to a perturbation by weakly damped, pronounced oscillations back to equilibrium, which are called relaxation oscillations (ROs) [51]. QW semiconductor lasers are typical class *B* lasers. Complex and particularly chaotic dynamical behavior only occurs if the laser is subject to an external perturbation, which adds an additional degree of freedom. This perturbation may consist of external optical injection or external optical feedback.

(iii) In **class A** lasers, the polarization as well as the carriers decay much faster than the field, and both may be eliminated adiabatically. The simple dynamics of class A lasers is well described by one differential equation for the field. External perturbations add one degree of freedom, which makes periodic or quasi periodic behavior possible. Typical representatives of class A lasers are gas lasers. Their cavity consists of highly refractive mirrors, which guarantees a long photon lifetime. Also QD semiconductor lasers can reach the dynamical stability of class A laser [6], which is discussed in the present and the next chapter.

In the dynamical equations (2.4) for the QD laser, the polarization has already been eliminated adiabatically. In contrast to QW lasers, the carrier lifetimes $\tau_e$ and $\tau_h$ of the optically active levels in QD lasers may be tuned by adapting the band structure. If the QD laser behaves like a class B or a class A laser, depends on the scaling of $\tau_e$ and $\tau_h$ with respect to the photon lifetime $\tau_{\mathrm{ph}} = 2\kappa$. (Note that in the dimensionless Eqs. (2.4) the photon lifetime is unity, i.e., the scaling of the dimensionless carrier lifetimes $t_e$ and $t_h$ with respect to unity has to be discussed). Figures 2.5a–c depict the turn-on dynamics of the QD laser for the three different band structures listed in Table 2.1, and additionally the limit of very large scattering rates is depicted in Fig. 2.5d. For this limit, the in-scattering rates of the shallow dot structure (fast rates) have been multiplied by a factor of $1 \times 10^4$.

The slow rates represent the class B limit of the equations. The carrier Eqs. (2.4b)–(2.4e) are multiplied by the small parameter $\gamma$, and the functions $F_b$ ($b = e$ for electrons and $b = h$ for holes), which contain the contributions of the scattering rates, are small enough to guarantee that the product $\gamma F_b \ll 1$ remains small. This means that the equations are of slow-fast type. As a consequence, the time series of the photon number $N_{\mathrm{ph}}$ (Fig. 2.5a left column) shows pronounced, weakly damped relaxation oscillations. In a linear theory, RO damping and frequency are determined by the eigenvalues of the Jacobien of Eqs. (2.4). The RO damping $\Gamma_{\mathrm{RO}}$ is determined by the eigenvalue, whose real part has the smallest absolute value, i.e., by the eigenvalue with the smallest decay rate. This eigenvalue is denoted as leading eigenvalue. Usually, the lasing fixed point is a stable focus and has a pair of complex conjugate leading eigenvalues $\tilde{\sigma}_{\pm} \equiv -\Gamma_{\mathrm{RO}} \pm i\omega_{\mathrm{RO}}$. The RO frequency $\omega_{\mathrm{RO}}$ is then given by the absolute value of the imaginary parts of these eigenvalues. For class B lasers, the damping is much smaller than the frequency ($\Gamma_{\mathrm{RO}} \ll \omega_{\mathrm{RO}}$) and oscillations can be observed. Figure 2.6a and b depict frequency $\omega_{\mathrm{RO}}$ and damping $\Gamma_{\mathrm{RO}}$ of the ROs, respectively, for the four different band structures of Fig. 2.5.

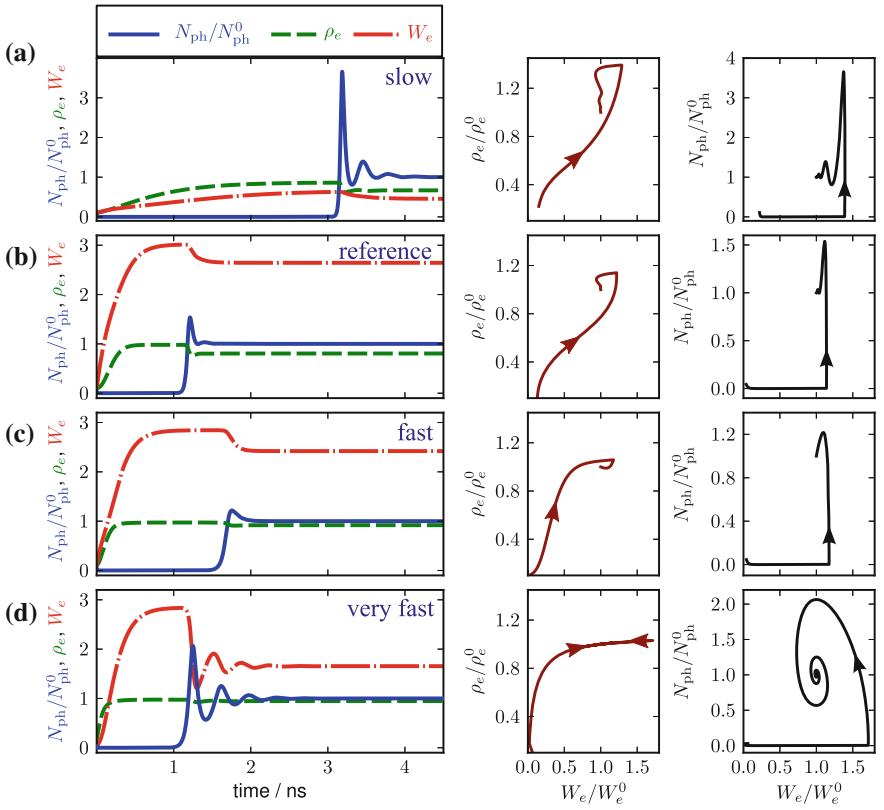


**Fig. 2.5** Turn-on dynamics for (**a**) slow, (**b**) reference, (**c**) fast, and (**d**) very fast sets of scattering rates studied in this work. *Left column* Time traces of the photon number $N_{\rm ph}$ (normalized to the steady state photon number $N_{\rm ph}^0$), the electronic occupation probability $\rho_e$, and the electron density in the carrier reservoir $W_e$. *Middle column* Phase space projections of the trajectories onto a plane spanned by $W_e$ and $\rho_e$ ($\rho_e^0$ and $W_e^0$ are the steady state values of $\rho_e$ and $W_e$, respectively). *Right column* Phase space projections of the trajectories onto a plane spanned by $W_e$ and $N_{\rm ph}$. Parameters $J = 2.5 \times J_{\rm th}$ and other parameters as in Table 2.2

RO frequency and damping were calculated from the eigenvalues of the linearized dynamical equations.

The fast rates represent the class A limit of the QD equations. Here, the product of $\gamma F_b$ is of order one, and the time scale separation breaks down.[2] As a result, the time series of $N_{\rm ph}$ in Fig. 2.5c shows an overdamped, relaxation free turn-on behavior. From Fig. 2.6, it can be seen that for $J < 2.2 J_{\rm th}$ ($J_{\rm th}$ denotes the pump current at lasing threshold) $\omega_{\rm RO}$ and $\Gamma_{\rm RO}$ are of the same order of magnitude, which makes oscillations impossible. For higher pump currents, the leading eigenvalue is real.

[2] In the following, the Landau symbol $\mathcal{O}$ is frequently used to describe the scaling of a quantity, e.g., '$\gamma F_b$ is of order one' may be written as $\gamma F_b = \mathcal{O}(1)$ [52].

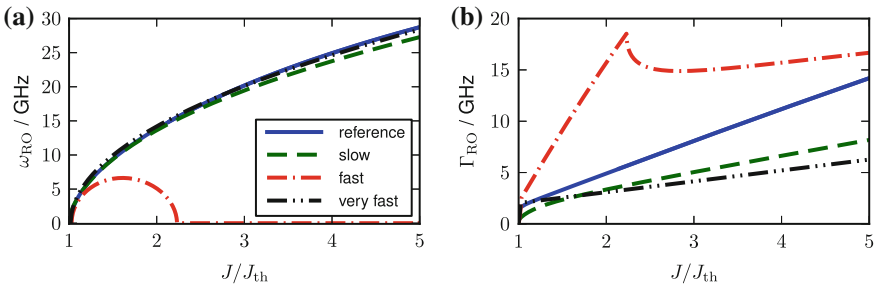


**Fig. 2.6** Frequency $\omega_{RO}$ (**a**) and damping $\Gamma_{RO}$ (**b**) of the RO oscillations versus the pump current $J$ (normalized to the pump current at lasing threshold $J_{th}$) as obtained from the numerically calculated eigenvalues for the four different band structures studied in this work. Parameters as in Table 2.3

The typical QD laser represented by the reference set of rates lies in between the class A and the class B limit of the equations. A time scale separation still exists, but the RO damping is much higher while the RO frequency is nearly the same as for the slow rates (see Fig. 2.6). This results in strongly suppressed ROs, which are depicted in the time series of Fig. 2.5b. Lingnau et al. studied RO frequency and damping of the shallow dot structure (energy differences of fast rates) by varying the lifetime of the electrons in the QDs ($\tau_e$) while keeping the ratio of electron and hole lifetime fixed [23, 53]. The authors observed that for the deep-dot structure, increasing the electronic lifetime from large values (corresponding to the slow rates) to smaller values first yields an increase of the RO damping. Then, the RO damping reaches a maximum, and eventually decays again. For the shallow-dot structure, the RO oscillations are completely damped out close to the maximum. Furthermore, the authors observed that the maximum of the RO damping for the deep dot structure appears when $\omega_{RO} \sim \tau_e^{-1}$. This corresponds to the observation that in the strongly damped regime, $\Gamma_{RO}$ and $\omega_{RO}$ are of the same order of magnitude, because the analytical formula for the RO damping of the reference rates reveals that the dominant contribution of the RO damping rate is given by the inverse lifetimes of the slower species, i.e.,

$$\Gamma_{RO} \sim \frac{\tau_e^{-1}}{2} \approx \frac{S_e^{in}}{2}.$$

This analytic expression for the RO damping was derived in [42] and will also be discussed in detail in Sect. 2.5.3. Generally, the electrons are slower than the holes, i.e., $\tau_e > \tau_h$, because the energetic distance between carrier reservoir and QD levels is larger for electrons due to their lower effective masses [28]. Thus, the dominant contribution to the RO damping is always given by the slower carrier type.

In Fig. 2.7, RO damping $\Gamma_{RO}$ (black dashed lines) and RO frequency $\omega_{RO}$ (red solid lines) of the shallow-dot QD laser (energy distances of fast set of scattering rates) are plotted with respect to the inverse electronic carrier lifetime $\tau_e^{-1}$. The carrier lifetimes $\tau_e$ and $\tau_h$ have been varied by multiplying the in-scattering rate $S_{e/h}^{in}$ with constant factors (indicated by green dots). Meanwhile, the pump current has been

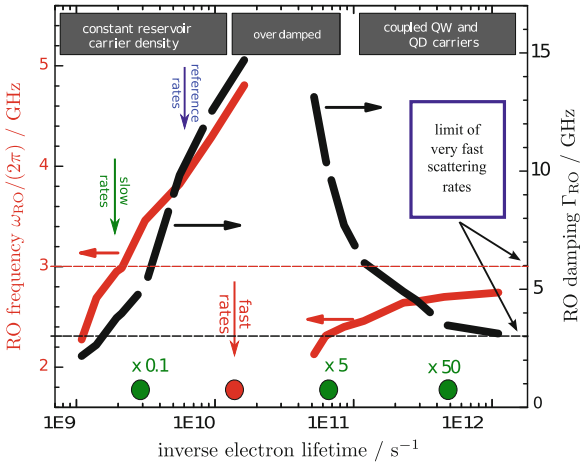


**Fig. 2.7** RO damping $\Gamma_{RO}$ and RO frequency $\omega_{RO}$ of the QD laser with respect to the inverse electronic carrier lifetime $\tau_e^{-1}$. Electron and hole lifetimes $\tau_e$ and $\tau_h$ have been varied by multiplying the in-scattering rates $S_{e/h}^{in}$ by constant factors. *Black* and *red dashed lines* label asymptotic values of $\omega_{RO}$ and $\Gamma_{RO}$ in the limit of very fast scattering rates ($\tau_{e/h} \to 0$), respectively. *Red*, *green*, and *blue arrows* indicate the values of $\tau_e$ for the reference and the fast set of rates, respectively. Parameters: $j = 2j_{th}$ and other parameters as in Table 2.3. Modified from [53]

adapted to keep a fixed pump level of $J = 2J_{th}$. The red dot and the red arrow denote the microscopically calculated scattering rates for the shallow dot structure, i.e., the fast set of scattering rates. It is located close to the maximum of the RO damping. Decreasing the scattering rates by multiplying with a factor smaller than unity, yields a strong decrease of the RO damping. Blue and green arrows indicate the inverse electronic lifetimes $\tau_e^{-1}$ as obtained from the deep dot structures of the reference rates and the slow rates, respectively. The RO damping decreases from the fast over the reference to the slow set of rates, as depicted in the time series of Fig. 2.5a–c. Increasing the scattering rates by multiplying with a factor larger than unity, i.e., decreasing $\tau_e^{-1}$, leads to a strong decrease of the RO damping, which results in a reappearance of the ROs. For very large values of the scattering rates, RO damping and RO frequency saturate to constant values denoted by the horizontal black dashed line and the horizontal red dashed line, respectively. The turn-on dynamics in the limit of very fast scattering rates is depicted in Fig. 2.5d.

For slow, reference, and fast scattering rates, the reservoir populations $W_e$ and $W_h$ vary very little above lasing threshold. This can be seen in the time series of Fig. 2.5a–c (left column) as well as in the phase space projections onto to $(W_e, N_{ph})$-plane (right column). From the latter, it can be seen that during the turn-on oscillations, $W_e$ remains close to its steady state value above threshold $W_e^0$. For not too large scattering rates, the reservoir is large enough to be hardly effected by the lasing process. Further, the middle column of Fig. 2.5a and b reveals that for the slow and the reference rates, the decay of $W_e$ is faster than the decay of $\rho_e$,

which expresses in a nearly vertical section at the end of the trajectory. In contrast, for the fast and very fast rates, $\rho_b$ decay faster than $W_b$, which expresses in nearly horizontal segment at the end of the trajectory (see middle column of Fig. 2.5c and d).

In contrast to slow, reference, and fast rates, the variation of the reservoir populations are more pronounced in the limit of very fast scattering rates ($F_b \to \infty$) depicted in Fig. 2.5d. The oscillations of $W_e$ observed in the time series (left panel) express in a projection of the trajectory onto the ($W_e$, $N_{\text{ph}}$)-plane in a spiraling motion towards the lasing fixed point, which is a stable focus (right panel). The reason is that the large scattering rates induce a carrier exchange fast enough for QD and reservoir carriers to be in quasi-equilibrium, which induces a strong coupling between reservoir and QD levels [23]. The laser system may now be described by dynamical equations for the dynamical variables $N_b^+ \equiv \rho_b + W_b$, which are the sums of the carrier population in the QD levels and in the carrier reservoir. This is discussed in detail in Sect. 3.7.4. The resulting equations are structurally similar to class B laser equations with a clear time scale separation between the photon and the slow carrier subsystem expressed by the small parameter $\gamma$. These findings are consistent with those obtained for a three variable rate equation model for a QD laser in [4].

## 2.5 Analytic Results

In the last section, it was discussed that the band structure of a QD laser has a strong impact on the damping of the ROs. In this section, analytical approximations of RO frequency and damping are introduced and compared to the corresponding expressions for a QW laser. Therefore, at first, a standard rate equation model for a conventional QW laser is discussed in Sect. 2.5.1. Then, in Sect. 2.5.2, the steady states of the QD laser are studied, before discussing the analytical expressions for RO frequency and damping in the limit of the reference and the slow sets of scattering rates (cf. Table 2.1) in Sects. 2.5.3 and 2.5.4, respectively. Furthermore, in Sect. 2.5.5 a reduced set of equations is derived that is valid in the limit of vanishing carrier lifetimes $\tau_e$ and $\tau_h$, i.e., in the limit of very fast scattering rates. Expressions for RO frequency and damping are then derived from the reduced set of equations, and compared to the QW laser. Table 2.4 summarizes the main results of this section. The analytical expressions for frequency $\omega^{\text{RO}}$ and RO damping $\Gamma^{\text{RO}}$ are expressed with respect to dimensionless time $t' = 2\kappa t$, which permits best to compare the expressions obtained for the reference rates ($\omega^{\text{ref}}$ and $\Gamma^{\text{ref}}$), for the slow rates ($\omega^{\text{S}}$ and $\Gamma^{\text{S}}$), the limit of very fast rates ($\omega^{\text{vf}}$ and $\Gamma^{\text{vf}}$), and for the QW model discussed in the next section ($\omega^{\text{QW}}$ and $\Gamma^{\text{QW}}$).

**Table 2.4** Analytic expressions for RO frequency $\omega^{\mathrm{RO}}$ and RO damping $\Gamma^{\mathrm{RO}}$ with respect to dimensionless time $t' \equiv 2\kappa t$ as obtained for reference, slow, and very fast rates as well as for the QW laser, respectively

| Rates/Laser | RO frequency ($\omega^{\mathrm{RO}}$) | RO damping ($\Gamma^{\mathrm{RO}}$) |
|---|---|---|
| Reference | $\omega^{\mathrm{ref}} \equiv \sqrt{\gamma r_w N_{\mathrm{ph}}^0}$ | $\Gamma^{\mathrm{ref}} \equiv \frac{\gamma}{2}\left[r_w N_{\mathrm{ph}}^0\left(\frac{t_h}{\gamma}+1\right)+t_e^{-1}+\rho_h^0\right]$ |
| Slow | $\omega^{\mathrm{S}} \equiv \sqrt{2\gamma r_w N_{\mathrm{ph}}^0}$ | $\Gamma^{\mathrm{S}} \equiv \Gamma^{\mathrm{S,QW}} + \frac{\gamma}{2}\left[g^{-1}+\frac{(t_e^{-1}+t_h^{-1})}{2}\right]$ with $\Gamma^{\mathrm{S,QW}} \equiv \frac{\gamma}{2}(1+2r_w N_{\mathrm{ph}}^0)$ |
| Very fast | $\omega^{\mathrm{vf}} \equiv \sqrt{\gamma r_w N_{\mathrm{ph}}^0\left(\frac{2+z_e+z_h}{(1+z_e)(1+z_h)}\right)}$ | $\Gamma^{\mathrm{vf}} \equiv \frac{\gamma r_w N_{\mathrm{ph}}^0}{2(1+z_e)(1+z_h)}\left[\begin{array}{c}2+z_h+z_e \\ +\rho_h^0(1+z_h)+\rho_e^0(1+z_e) \\ +c\left[\begin{array}{c}W_e^0 z_h(1+z_e) \\ +W_h^0 z_e(1+z_h)\end{array}\right]\end{array}\right]$ |
| QW laser | $\omega^{\mathrm{QW}} \equiv \sqrt{2\gamma^{\mathrm{QW}} r^{\mathrm{QW}} N_{\mathrm{ph}}^0}$ | $\Gamma^{\mathrm{QW}} \equiv \gamma^{\mathrm{QW}} \frac{(1+2r^{\mathrm{QW}} N_{\mathrm{ph}}^0)}{2}$ |

### 2.5.1 Quantum Well Laser

In this section, analytical expressions for RO frequency and damping for a rate equation model for a conventional, single-mode, class B QW laser model [54, 55] are derived. The QW rate equations are given by

$$\frac{d\mathcal{E}}{dt} = \frac{1}{2}\left[G_n(n-n_{\mathrm{tr}}) - \frac{1}{\tau_{\mathrm{ph}}}\right]\mathcal{E}, \tag{2.10a}$$

$$\frac{dn}{dt} = \frac{j}{e_0} - \frac{n}{\tau_c} - G_n(n-n_{\mathrm{tr}})(\mathcal{E})^2. \tag{2.10b}$$

Here, $\mathcal{E}$ is the slowly varying amplitude of the electrical field, which is normalized such that $\mathcal{E}^2 = N_{\mathrm{ph}}$, and $n$ is the carrier density. The linear gain coefficient is denoted by $G_N$, $n_{\mathrm{tr}}$ is the transparency density of carriers, $j$ is the pumping current density, $e_0$ the elementary charge, and $\tau_{\mathrm{ph}}$ and $\tau_c$ are the photon and carrier lifetimes, respectively. Equating the left hand sides of Eqs. (2.10) to zero, the non-zero intensity steady state ($N_{\mathrm{ph}} \neq 0$) is

$$n^0 = n_{\mathrm{tr}} + \frac{1}{G_n \tau_{\mathrm{ph}}}, \tag{2.11}$$

$$(\mathcal{E}^0)^2 = \frac{1}{G_n(n^0-n_{\mathrm{tr}})}\left(\frac{j}{e_0} - \frac{n^0}{\tau_c}\right), \tag{2.12}$$

where the superscript $(\cdot)^0$ is used to mark steady state values. From the linearized equations, the characteristic equation for the growth rate $\tilde{\sigma}$ is the determined as

$$\tilde{\sigma}^2 + \left(\frac{1}{\tau_c} + G_n(\mathcal{E}^0)^2\right)\tilde{\sigma} + \frac{1}{\tau_{\text{ph}}} G_n(\mathcal{E}^0)^2 = 0. \tag{2.13}$$

In order to properly define the RO frequency and its damping rate, we take advantage of the fact that $\tau_{\text{ph}} \ll \tau_c$, i.e., that the photon subsystem is much faster than the one of the carriers. The roots of the quadratic equation then take the form

$$\tilde{\sigma} = -\Gamma_{\text{RO}}^{\text{QW}} \pm i\omega_{\text{RO}}^{\text{QW}}, \tag{2.14}$$

where

$$\Gamma_{\text{RO}}^{\text{QW}} \equiv \frac{1}{2}\left(\frac{1}{\tau_s} + G_n(\mathcal{E}^0)^2\right), \tag{2.15}$$

$$\omega_{\text{RO}}^{\text{QW}} \equiv \sqrt{\frac{G_n}{\tau_{\text{ph}}}(\mathcal{E}^0)^2 - \left(\Gamma_{\text{RO}}^{\text{QW}}\right)^2} \approx \sqrt{\frac{G_n}{\tau_{\text{ph}}} N_{\text{ph}}^0} \tag{2.16}$$

are defined as the RO damping rate and RO frequency of the solitary laser, respectively. They are the main quantities of a laser that can be easily measured experimentally.

In order to determine asymptotic approximations, the rate equations have to be reformulated in dimensionless form. The simplest way is to measure time in units of the photon lifetime by introducing

$$t' \equiv t/\tau_{\text{ph}}. \tag{2.17}$$

Furthermore, introducing the new dimensionless dependent inversion $\rho_{\text{inv}}$ defined by

$$\rho_{\text{inv}} \equiv \frac{1}{2}\left[G_n(n - n_{\text{tr}})\tau_{\text{ph}} - 1\right] \tag{2.18}$$

allows to reduce the number of parameters.

Inserting Eqs. (2.17) and (2.18) into Eqs. (2.10a) and (2.10b), yields

$$\frac{d\mathcal{E}}{dt'} = \rho_{\text{inv}}\mathcal{E}, \tag{2.19a}$$

$$\frac{d\rho_{\text{inv}}}{dt'} = \gamma^{\text{QW}}\left[P - \rho_{\text{inv}} - r^{\text{QW}}(1 + 2\rho_{\text{inv}})\mathcal{E}^2\right], \tag{2.19b}$$

where the time scale separation $\gamma^{\text{QW}}$, the pump $P$, and $r^{\text{QW}}$[3] are defined by

[3] Note that often in the literature (cf. [48, 49, 56, 57]) a rescaled field amplitude $R \equiv \sqrt{r^{\text{QW}}}\mathcal{E}$ is introduced, such that the rescaled intensity $I \equiv R^2$ is of $\mathcal{O}(1)$. However, to compare the findings of this section with those derived for the QD model in the next sections, $\mathcal{E}^2 = N_{\text{ph}}$ is used.

$$\gamma^{\mathrm{QW}} \equiv \frac{\tau_{\mathrm{ph}}}{\tau_c},\ P \equiv \frac{G_n \tau_{\mathrm{ph}} \tau_c}{2e_0}\,(j - j_{\mathrm{th}}),\quad \text{where}\quad j_{\mathrm{th}} \equiv e_0 \left(\frac{n_{\mathrm{tr}}}{\tau_c} + \frac{1}{G_n \tau_{\mathrm{ph}} \tau_c}\right)$$
$$\text{and}\quad r^{\mathrm{QW}} \equiv \frac{\tau_c G_n}{2}. \tag{2.20}$$

The non-zero intensity steady state is given by

$$\rho^0_{\mathrm{inv}} = 0 \text{ and } N^0_{\mathrm{ph}} \equiv (\mathcal{E}^0)^2 = P/r^{\mathrm{QW}}. \tag{2.21}$$

The rescaled inversion $\rho^0_{\mathrm{inv}}$ is zero above lasing threshold, which is known as gain-clamping [58], and $N^0_{\mathrm{ph}}$ increases linearly with the pump $P \sim j - j_{\mathrm{th}}$. The characteristic equation for the growth rate $\sigma$ is given by

$$\sigma^2 + \gamma^{\mathrm{QW}}(1 + 2r^{\mathrm{QW}} N^0_{\mathrm{ph}})\sigma + 2\gamma^{\mathrm{QW}} r^{\mathrm{QW}} N^0_{\mathrm{ph}} = 0. \tag{2.22}$$

Provided $\gamma^{\mathrm{QW}}$ is sufficiently small, the roots of Eq. (2.22) are complex conjugate. The dimensionless RO damping rate and the RO frequency (in units of time $t'$) are then defined from the imaginary and real part of these roots. We obtain

$$\Gamma^{\mathrm{QW}} \equiv \gamma^{\mathrm{QW}} \frac{(1 + 2r^{\mathrm{QW}} N^0_{\mathrm{ph}})}{2} = \gamma^{\mathrm{QW}} \frac{(1 + 2P)}{2}, \tag{2.23a}$$
$$\omega^{\mathrm{QW}} \equiv \sqrt{2\gamma^{\mathrm{QW}} r^{\mathrm{QW}} N^0_{\mathrm{ph}} - (\Gamma^{\mathrm{QW}})^2} \approx \sqrt{2\gamma^{\mathrm{QW}} r^{\mathrm{QW}} N^0_{\mathrm{ph}}} \text{ as } \gamma^{\mathrm{QW}} \to 0. \tag{2.23b}$$

Note that the RO damping scales like $\gamma^{\mathrm{QW}}$ and is thus much smaller than the RO frequency, which scales like $\sqrt{\gamma^{\mathrm{QW}}}$. This is the reason for the pronounced relaxation oscillations observed in class B lasers.

The same dimensionless time $t' \equiv t/\tau_{\mathrm{ph}}$ is used in the analysis of the QD rate equations of the solitary laser discussed in the remainder of this section as well as in the analysis of the QD laser under optical injection (Chap. 3) and the analysis of the QD laser subject to optical feedback (Chap. 4). Furthermore, the dynamic equations are formulated such that a small time scale separation parameter $\gamma$ multiplies the right hand side of the carrier equations (cf. Eqs. (2.4)).

### *2.5.2 Steady States of Solitary Quantum Dot (QD) Laser*

Now, the solitary QD laser Eqs. (2.4) are analyzed starting with the steady states. For the subsequent analysis, the spontaneous emission in the field Eqs. (2.4) is neglected by setting $d = 0$. Equating to zero the right hand sides of Eqs. (2.4), yields the steady state relations

$$0 = \rho^0_{\rm inv} N^0_{\rm ph}, \tag{2.24a}$$

$$0 = \gamma\Big[F_e(\rho^0_e, \rho^0_h, W^0_e, W^0_h) - r_w(\rho^0_e + \rho^0_h - 1)N^0_{\rm ph} - \rho^0_e\rho^0_h\Big], \tag{2.24b}$$

$$0 = \gamma\Big[F_h(\rho^0_e, \rho^0_h, W^0_e, W^0_h) - r_w(\rho^0_e + \rho^0_h - 1)N^0_{\rm ph} - \rho^0_e\rho^0_h\Big], \tag{2.24c}$$

$$0 = \gamma\Big[J - F_e(\rho^0_e, \rho^0_h, W^0_e, W^0_h) - cW^0_eW^0_h\Big], \tag{2.24d}$$

$$0 = \gamma\Big[J - F_h(\rho^0_e, \rho^0_h, W^0_e, W^0_h) - cW^0_eW^0_h\Big], \tag{2.24e}$$

where steady state values of dynamical variables are denoted by superscript $(\cdot)^0$. Equation (3.18) shows that above threshold ($N_{\rm ph} \neq 0$) the inversion is clamped to zero

$$\rho^0_{\rm inv} \equiv \frac{1}{2}\Big[g(\rho^0_e + \rho^0_h - 1) - 1\Big] = 0, \tag{2.25}$$

which is known as gain-clamping [56]. Next, the steady state of the photon number may be expressed in terms of the carrier populations and the pump current, by inserting Eq. (2.24d) into Eq. (2.24b)

$$N^0_{\rm ph} = \frac{g}{r_w}\left(J - cW^0_eW^0_h - \rho^0_e\rho^0_h\right) \approx \frac{g}{r_w}(J - J_{\rm th}) = \frac{g}{r_w}\left(\frac{J}{J_{\rm th}} - 1\right)J_{\rm th}. \tag{2.26}$$

Here, the gain-clamping of Eq. (2.25) has been used to write $\rho^0_e + \rho^0_h - 1 = g^{-1}$. The approximation in the last equality of Eq. (2.26) is based on the assumption that the product of the carrier densities does not vary significantly above threshold, which permits to introduce the threshold current of the solitary laser as

$$J_{\rm th} \equiv cW^{\rm th}_eW^{\rm th}_h - \rho^{\rm th}_e\rho^{\rm th}_h, \tag{2.27}$$

where quantities with superscript $(\cdot)^{\rm th}$ are taken at the lasing threshold of the solitary laser. Equation (2.26) expresses the linear increase of the photon number with the current observed above threshold [45, 59].

Further, with the help of the carrier conservation relation of Eq. (2.9), expressions of $\rho^0_e$ and $\rho^0_h$ in terms of the reservoir populations $W^0_e$ and $W^0_h$ are obtained from Eq. (2.25), which read

$$\rho^0_e = \frac{1}{2}\left[\frac{1+g}{g} + W^0_h - W^0_e\right] \quad \text{and} \quad \rho^0_h = \frac{1}{2}\left[\frac{1+g}{g} - W^0_h + W^0_e\right]. \tag{2.28}$$

Eventually, the steady states of the reservoir populations $W^0_e$ and $W^0_h$ can be calculated by inserting Eqs. (2.28) into Eqs. (2.24d) and (2.24e), and the solving self-consistently for $W^0_e$ and $W^0_h$. This has to be done numerically, because $F_e$ and $F_h$ are nonlinear functions of $W^0_e$ and $W^0_h$ (see Eqs. (2.6)).

### 2.5.3 QD Laser: RO Frequency and Damping for the Reference Rates

In the limit of the reference and the slow set of scattering rates (cf. Table 2.1), analytical expression for RO frequency and damping of the QD laser have been derived by Lüdge et al. in Ref. [42]. In this and the next subsection, the resulting expression are discussed for the slow and the reference rates, respectively. The asymptotic methods needed to derive these expression are introduced in Sect. 3.6, and eventually the formulas for RO damping and frequency (cf. Table 2.4) are retrieved from the eigenvalues of the laser under optical injection in Sect. 3.8.

With respect to the dimensionless time $t' \equiv (2\kappa)^{-1}t$, RO frequency and damping of the solitary laser are given for the set of reference scattering rates by

$$\omega^{\text{ref}} \equiv \sqrt{\gamma r_w N_{\text{ph}}^0} \approx \sqrt{\gamma g(J - J_{\text{th}})} \quad \text{and} \tag{2.29a}$$

$$\begin{aligned}\Gamma^{\text{ref}} &\equiv \frac{\gamma}{2}\left[r_w N_{\text{ph}}^0\left(\frac{t_h}{\gamma}+1\right)+t_e^{-1}+\rho_h^0\right] \\ &\approx \frac{\gamma}{2}\left[g(J-J_{\text{th}})\left(\frac{t_h}{\gamma}+1\right)+t_e^{-1}+\rho_h^0\right],\end{aligned} \tag{2.29b}$$

respectively. In the approximations of Eqs. (2.29), a linear dependence of $N_{\text{ph}}^0$ on the pump current was assumed (see Eq. (2.26)). Eventually, we obtain for the RO frequency $\omega_{\text{RO}}^{\text{ref}} \equiv 2\kappa\omega^{\text{ref}}$ and damping $\Gamma_{\text{RO}}^{\text{ref}} \equiv 2\kappa\Gamma^{\text{ref}}$ in terms of physical time $t$

$$\omega_{\text{RO}}^{\text{ref}} = 2\kappa\sqrt{\gamma r_w N_{\text{ph}}^0} \approx 2\kappa\sqrt{\gamma g(J - J_{\text{th}})}, \tag{2.30a}$$

$$\begin{aligned}\Gamma_{\text{RO}}^{\text{ref}} &= \kappa\gamma\left[2r_w N_{\text{ph}}^0\left(\frac{W\tau_h}{\gamma}+\frac{1}{2}\right)+\frac{1}{W\tau_e}+\rho_h^0\right] \\ &\approx \kappa\gamma\left[2g(J-J_{\text{th}})\left(\frac{W\tau_h}{\gamma}+\frac{1}{2}\right)+\frac{1}{W\tau_e}+\rho_h^0\right].\end{aligned} \tag{2.30b}$$

Figure 2.8a and b depict RO frequency and damping as obtained from the numerically calculated eigenvalues of the full system (full black lines) and from the analytical approximations (2.30) (blue dashed lines). The RO frequency clearly shows the square-root like scaling with the pump current as predicted by Eq. (2.30a), and $\Gamma_{\text{RO}}^{\text{ref}}$ scales in very good approximation linearly with the pump current. Further, for low pump currents, the $\kappa\gamma/(W\tau_e)$-term (green dashed line in Fig. 2.8b) constitutes the dominant contribution to the RO damping. This permits to conclude that for low pump currents the slower carrier type, i.e., the electrons, dominate the turn-on damping [42], while, for pump currents high above threshold, the first two terms in the rectangular brackets of Eq. (2.30b) become more important. Next, the expression (2.29a) for the RO frequency of the QD laser is compared to the corresponding expression (2.23b) for the QW laser. It can be seen that the RO frequency of the QD laser is by a factor $1/\sqrt{2}$ lower than for the QW laser if for QD and QW the same

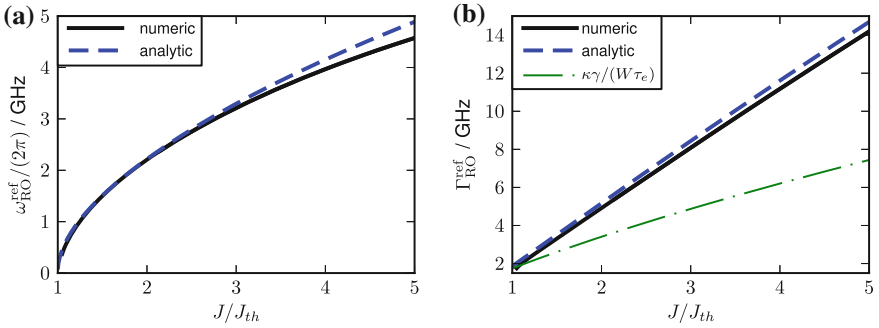


**Fig. 2.8** Comparison of RO frequency $\omega_{RO}^{ref}$ (**a**) and RO damping $\Gamma_{RO}^{ref}$ (**b**) calculated numerically from the eigenvalues of the full system (*black solid lines*) with their analytical approximations of Eqs. (2.30a) and (2.30b) (blue dashed lines). The thin *dash-dotted green line* in (**b**) marks the dominant contribution $\kappa\gamma/(W\tau_e)$ of the RO damping. Parameters: reference rates and other parameters as in Table 2.3

time scale separation ($\gamma^{QW} = \gamma$), the same ratio of the Einstein factors ($r^{QW} = r_w$), and the same steady state photon number $N_{ph}^0$ are assumed.

### 2.5.4 QD Laser: RO Frequency and Damping for the Slow Rates

For the slow set of scattering rates of Table 2.1, RO frequency and damping read in units of time $t' = (2\kappa)^{-1}t$

$$\omega^S \equiv \sqrt{2\gamma r_w N_{ph}^0} \approx \sqrt{2\gamma g(J - J_{th})}, \tag{2.31a}$$

$$\Gamma^S \equiv \Gamma^{S,QW} + \frac{\gamma}{2}\left[g^{-1} + \frac{(t_e^{-1} + t_h^{-1})}{2}\right], \tag{2.31b}$$

where we have introduced

$$\Gamma^{S,QW} \equiv \frac{\gamma}{2}(1 + 2r_w N_{ph}^0) \approx \frac{\gamma}{2}[1 + 2g(J - J_{th})], \tag{2.32}$$

The contribution $\Gamma^{S,QW}$ corresponds to the RO damping of the QW laser (cf. Eq. (2.23a)) for $\gamma^{QW} = \gamma$ and $r^{QW} = r_w$. Furthermore, the linear dependence of $N_{ph}^0 \approx g/(r_w)(J - J_{th})$ on the pump current $J$ (see Eq. (2.26)) was used. Finally, in units of the physical time $t = 2\kappa t'$ the damping rate reads

$$\omega_{RO}^S \equiv 2\kappa\sqrt{2\gamma r_w N_{ph}^0} \approx 2\kappa\sqrt{2\gamma g(J - J_{th})}, \tag{2.33a}$$

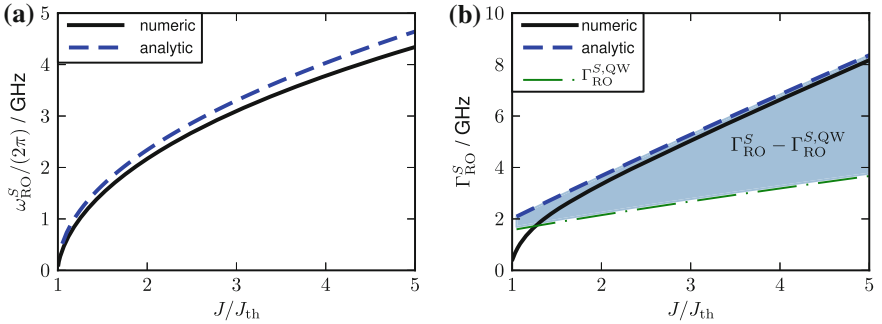


**Fig. 2.9** Comparison of RO frequency $\omega_{\rm RO}^{\rm S}$ (**a**) and RO damping $\Gamma_{\rm RO}^{\rm S}$ (**b**) as obtained numerically from the eigenvalues of the full system (*black lines*) with their analytical approximations of Eqs. (2.33a) and (2.33b) (*blue dash dotted lines*). The QW contribution $\Gamma_{\rm RO}^{\rm S,QW}$ of Eq. (2.34) is marked by a *green dash-dotted line* in (**b**), and the *blue shaded region* in (**b**) marks the difference of $\Gamma_{\rm RO}^{\rm S}$ and $\Gamma_{\rm RO}^{\rm S,QW}$. Parameters: slow rates and other parameters as in Table 2.3

$$\Gamma_{\rm RO}^{\rm S} \equiv \Gamma_{\rm RO}^{\rm S,QW} + \kappa\gamma\left[g^{-1} + \frac{1}{W}\left(\frac{\tau_e^{-1} + \tau_h - 1}{2}\right)\right], \tag{2.33b}$$

where the QW contribution to the damping rate $\Gamma_{\rm RO}^{\rm S,QW}$ is given by

$$\Gamma_{\rm RO}^{\rm S,QW} \equiv \kappa\gamma\left[1 + 2r_w N_{\rm ph}^0\right] \approx \kappa\gamma\,[1 + 2g(J - J_{\rm th})]. \tag{2.34}$$

Figure 2.9a and b depict RO frequency and damping as obtained from the eigenvalues of the full system (full black lines) and from the analytical approximations (2.33) (dashed blue lines), respectively. As in the limit of the reference rates, the RO frequency clearly shows the square-root like scaling with the pump current as predicted by Eq. (2.33a). The RO damping $\Gamma_{\rm RO}^{\rm S}$ (see Eq. (2.33b)) scales for $J \gtrsim 2J_{\rm th}$ linearly with the pump current. For the QW contribution $\Gamma_{\rm RO}^{\rm S,QW}$, this can be seen directly from Eq. (2.34), and the term in the rectangular brackets in Eq. (2.33b) scales nearly linearly with the pump current, because the constant term proportional to $g^{-1}$ is negligible, and the inverse carrier lifetimes $\tau_e^{-1}$ and $\tau_h^{-1}$ increase nearly linearly with $J$. To see this, note that for the slow set of scattering rates, the in- and out-scattering rates $S_{e/h}^{\rm in/out}$ for both, electrons and holes, are similar to the electronic scattering rates for the reference set of rates. The latter are depicted in Fig. 2.2a and b, respectively. From Fig. 2.2b, we see that the out-scattering rates are negligible, which yields $\tau_{e,h}^{-1} \approx S_{e/h}^{in}$, and from Fig. 2.2a, we note that well above threshold, i.e., to the right of the gray dashed line denoting the steady state of $w_e$ for $J = 1.5J_{\rm th}$, the in-scattering rates scale nearly linearly with the pump current.

The RO frequency is exactly the same as for a QW laser (cf. Eq. (2.23b)) with the same time scale separation ($\gamma^{\rm QW} = \gamma$) and the same ratio of the Einstein factors ($r^{\rm QW} = r_w$). It would thus be by a factor $\sqrt{2}$ higher than in the limit of the

reference rates (see Eq. (2.30b)) if both lasers had the same steady state photon number $N_{\mathrm{ph}}^{0}$ at the same pump level $J/J_{\mathrm{th}}$ (see last equality in Eq. (2.26)). However, comparing the pump dependence of $\omega_{\mathrm{RO}}^{\mathrm{S}}$ in Fig. 2.9a with the pump dependence of $\omega_{\mathrm{RO}}^{\mathrm{ref}}$ in Fig. 2.8, we see that the higher photon number in the case of the reference rates overcompensates the factor $\sqrt{2}$, and consequently, $\omega_{\mathrm{RO}}^{\mathrm{ref}}$ is even slightly higher than $\omega_{\mathrm{RO}}^{\mathrm{S}}$.

As already discussed in the introductory Sect. 2.2, the damping is much higher in the limit of the reference rates than in the limit of the slow rates, which may be seen by comparing Fig. 2.8b with Fig. 2.9b. The formula (2.33b) for the damping of the slow rates contains two contributions. The first term $\Gamma_{\mathrm{RO}}^{\mathrm{S,QW}}$ corresponds to the damping rate of a QW laser having the same time scale separation ($\gamma^{\mathrm{QW}} = \gamma$), the same ratio of the Einstein factors ($r^{\mathrm{QW}} = r_w$), and the same steady state photon number (see Eq. (2.23a)). The second term contains the contribution of the carrier lifetimes $\tau_e$ and $\tau_h$ in the QD levels and thus describes the impact of the band structure on the RO damping. Since electron and hole lifetimes are similar for the set of slow rates (see Table 2.1), they enter symmetrically into the expression (2.33b). Further, from Table 2.1, it can be seen that $\tau_e$ and $\tau_h$ are now similar to the electronic lifetime in the limit of the reference rates. This is why they contribute in the same way to $\Gamma_{\mathrm{RO}}^{\mathrm{S}}$ (see Eq. (2.33b)) than the electronic lifetime $\tau_e$ contributes to $\Gamma_{\mathrm{RO}}^{\mathrm{ref}}$ (see Eq. (2.30b)). The bluish shaded region in Fig. 2.9 marks the difference between the full damping rate $\Gamma_{\mathrm{RO}}^{\mathrm{S}}$ and its QW contribution $\Gamma_{\mathrm{RO}}^{\mathrm{S,QW}}$. Thus, it describes the impact of the band structure. The difference increases with the pump current, because $\tau_e^{-1}$ and $\tau_h^{-1}$ increase faster with the pump current (cf. Fig. 2.3) than the steady state of the photon number $N_{\mathrm{ph}}^{0}$.

### 2.5.5 QD Laser: Limit of Very Fast Scattering Rates

The limit of very fast scattering rates is described by the limit $F_b \to \infty$ ($b = e$ for electrons and $b = h$ for holes) of the dynamical equations (2.4). In this regime, the carrier lifetimes $\tau_b$ in the QD levels vanish, and the carrier exchange is fast enough to ensure that QDs and carrier reservoir remain in quasi-equilibrium during the turn-on process. This results in an enhanced coupling between reservoir and QD variables, which is best taken into account by introducing the new variables $N_b^+$ and $N_b^-$

$$N_b^+ \equiv \rho_b + W_b \quad \text{and} \quad N_b^- \equiv \rho_b - W_b. \tag{2.35}$$

Rewriting $\rho_b$ and $W_b$ in terms of the new variables, yields

$$\rho_b = \frac{N_b^+ + N_b^-}{2} \quad \text{and} \quad W_b = \frac{N_b^+ - N_b^-}{2}. \tag{2.36}$$

Further, for the subsequent analysis, it is convenient that the dynamical variables are all $\mathcal{O}(1)$, which simplifies their comparison to the small parameter $\gamma$ describing the time scale separation. Therefore, we rescale the photon number $N_{\mathrm{ph}}$[4] with respect to its steady state value $N_{\mathrm{ph}}^0$ (see Eq. (2.26)) by introducing $N_{\mathrm{ph}} = N_{\mathrm{ph}}^0 R^2$, where $R$ is $\mathcal{O}(1)$. The dynamical equations (2.4) then read in the new coordinates

$$R' = \rho_{\mathrm{inv}} R, \tag{2.37a}$$

$$(N_e^+)' = (N_h^+)' = \gamma\Big[J - r_{\mathrm{ph}}(\rho_e + \rho_h - 1)R^2 - \rho_e\rho_h - cW_eW_h\Big], \tag{2.37b}$$

$$(N_e^-)' = \gamma\Big[-J + 2F_e - r_{\mathrm{ph}}(\rho_e + \rho_h - 1)R^2 - \rho_e\rho_h + cW_eW_h\Big], \tag{2.37c}$$

$$(N_h^-)' = \gamma\Big[-J + 2F_h - r_{\mathrm{ph}}(\rho_e + \rho_h - 1)R^2 - \rho_e\rho_h + cW_eW_h\Big], \tag{2.37d}$$

where $r_{\mathrm{ph}} \equiv r_w N_{\mathrm{ph}}^0$ has been introduced. Due to the carrier conservation (2.8), which reads in these coordinates as $(N_e^+)' = (N_h^+)'$, the dynamical variables $N_e^+$ and $N_h^+$ have the same dynamics, and additionally one carrier variable may be eliminated, i.e, expressed in terms of the others. For the set of very fast scattering rates, we may assume that the terms $F_b \equiv s_b^{\mathrm{in}} - (s_b^{\mathrm{in}} + s_b^{\mathrm{out}})\rho_b$ expressing the impact of the Coulomb scattering rates are at least $\mathcal{O}(\gamma^{-2})$ large, which justifies an adiabatic elimination of $N_e^-$ and $N_h^-$, i.e, to assume $(N_e^-)' = (N_h^-)' = 0$. Equating to zero the right hand sides of Eqs. (2.37c) and (2.37d), and employing the definitions of the $F_b$'s, the QD populations can be expressed as

$$\rho_b = s_b^{\mathrm{in}} t_b - \frac{t_b}{2}\{J + r_{\mathrm{ph}}(\rho_e + \rho_h - 1)R^2 + \rho_e\rho_h - cW_eW_h\},$$

where we have used the dimensionless carrier lifetimes $t_b \equiv (s_b^{\mathrm{in}} + s_b^{\mathrm{out}})^{-1}$, which are at least $\mathcal{O}(\gamma^2)$ small. Since the terms in the curly brackets are all $\mathcal{O}(1)$, they constitute only a small correction to the first term, and the above equation can be written as

$$\rho_b = t_b s_b^{\mathrm{in}} + \mathcal{O}(\gamma^2). \tag{2.38}$$

In- and out-scattering rates are related by the detailed balance relation (2.2) [5], which reads in its dimensionless form (see also Appendix A)

$$s_b^{\mathrm{out}} = s_b^{\mathrm{in}} e^{-\frac{\Delta E_b}{k_{\mathrm{bo}}\mathcal{T}}}\left[e^{c_b W_b} - 1\right]^{-1}, \tag{2.39}$$

where the coefficients $c_b \equiv 2N^{\mathrm{QD}}/(D_b k_{\mathrm{bo}}\mathcal{T})$ were introduced. Inserting Eq. (2.39) into Eq. (2.38), the $\rho_b$ 's can be expressed in terms of the reservoir populations $W_b$ as

[4] Typically, $N_{\mathrm{ph}} = \mathcal{O}(10^4)$, which implies that the product of $r_w N_{\mathrm{ph}}^0$ is a $\mathcal{O}(1)$.

$$\rho_b(W_b) = t_b s_b^{\text{in}} = \frac{1}{1 + s_b^{\text{out}}/s_b^{\text{in}}} = \left(1 + e^{-\frac{\Delta E_b}{k_{\text{bo}} T}} \left[e^{c_b W_b} - 1\right]^{-1}\right)^{-1}, \tag{2.40}$$

which is valid up to $\mathcal{O}(\gamma^2)$. From the above formula, we see that in leading order $\rho_e$ is only a function of $W_e$, and that the same holds for the holes. Thus, the coupling to the other carrier type is at least $\mathcal{O}(\gamma^2)$ small, and may be neglected. This permits to express the reservoir populations $W_b$ in terms of $\rho_b$ by inverting Eq. (2.40)

$$W_b(\rho_b) = \frac{1}{c_b} \ln\left(1 + e^{-\frac{\Delta E_b}{k_{\text{bo}} T}} \frac{\rho_b}{1 - \rho_b}\right). \tag{2.41}$$

Instead of expressing the right hand sides of the dynamical equations (2.37a) and (2.37b) in terms of the $N_b^{\pm}$ s, we can use Eq. (2.41) to write $N_e^+ = \rho_e + W_e(\rho_e)$ as a function of $\rho_e$. This permits to formulate the right hand side of Eq. (2.37b) as

$$(N_e^+)' = \frac{d}{dt'}\left(\rho_e + W_e(\rho_e)\right) = (1 + \partial_{\rho_e} W_e)\rho_e'. \tag{2.42}$$

Employing the above equation, the dynamical equations (2.4) simplify in the limit of very large scattering rates ($F_b \to \infty$) as

$$R' = \rho_{\text{inv}} R, \tag{2.43a}$$

$$\rho_e' = \frac{\gamma}{1 + z_e}\left[J - r_{\text{ph}}(\rho_e + \rho_h - 1)R^2 - \rho_e \rho_h - c W_e W_h\right], \tag{2.43b}$$

where the abbreviations

$$z_b \equiv \partial_{\rho_b}\big|_{\rho_b^0} W_b = \left[c_b(1 - \rho_b)\left(e^{\frac{\Delta E_b}{k_{\text{bo}} T}}(1 - \rho_b) + \rho_b\right)\right]^{-1} \tag{2.44}$$

have been introduced. In Eqs. (2.43) the hole populations $\rho_h$ and $W_h(\rho_h)$ are functions of $\rho_e$. For a given value of $\rho_e$, the electronic population in the reservoir $W_e$ can be calculated from Eq. (2.41) for $b = e$. Furthermore, the occupation probability of the hole level $\rho_h$ can be calculated by inserting Eq. (2.41) for $b = h$ into the carrier conservation (2.9), which yields

$$\rho_h + W_h(\rho_h) = \rho_e + W_e(\rho_e). \tag{2.45}$$

The above equation can then be solved for $\rho_h$, and eventually, $W_h$ can be calculated from Eq. (2.41) for $b = h$.

The dynamical equations (2.43) describe a typical slow-fast system consisting of a fast optical subsystem (Eq. (2.43a)) and a slow carrier subsystem (Eq. (2.43b)). The time scale separation is expressed by the small parameter $\gamma$. (Note that $z_e$ and the terms in the brackets in Eq. (2.43b) are all $\mathcal{O}(1)$.) Thus, from Eqs. (2.43), we would expect the turn-on dynamics of the QD laser to be similar to the one of a

class B QW laser. That this is actually the case can be seen from the time series in Fig. 2.5d, which shows pronounced, weakly damped ROs that are typical for class B QW lasers.

In the remainder of this section, at first, the steady states of Eqs. (2.43) are discussed, and then analytical expression for frequency and damping of the ROs are derived.

### Steady States

The steady states are calculated from Eqs. (2.43) by equating to zero their right hand sides, which yields

$$0 = \rho_{\mathrm{inv}} R^0, \tag{2.46a}$$

$$0 = \frac{\gamma}{1+z_e}\left[J - r_{\mathrm{ph}}(\rho_e + \rho_h - 1)\left(R^0\right)^2 - \rho_e\rho_h - cW_eW_h\right]. \tag{2.46b}$$

By definition, the steady state of $R$ above leasing threshold is given by $R^0 = 1$. Since the optical steady state equation (2.46a) is the same as for the full system (see Eq. (2.4a)) with $R^0$ replaced by $N_{\mathrm{ph}}^0$, the gain-clamping relation $\rho_{\mathrm{inv}}^0 = 0$ remains valid (see Eq. (2.25)). From the carrier equation (2.46b), we then see that also the expression (2.26) for $N_{\mathrm{ph}}^0$ as a function of the carrier populations remains valid. The steady state $\rho_e^0$ of $\rho_e$ may be obtained by at first calculating the steady state $\rho_h^0$ of $\rho_h$ as a function of $\rho_e^0$ from Eq. (2.45), inserting then the resulting expression for $\rho_h^0 = \rho_h(\rho_e^0)$ into Eq. (2.25), and then solving for $\rho_e^0$. Subsequently, $\rho_h^0$ is calculated by inserting $\rho_e^0$ back into Eq. (2.45), and eventually, the steady states of the reservoir populations $W_e^0$ and $W_h^0$ can be calculated from Eq. (2.41).

### RO Frequency and Damping in the Limit of Very Fast Scattering Rates

For the linearization of the dynamical equations (2.43), the partial derivatives of $\rho_h$ and $W_h$ with respect to $\rho_e$ have to be calculated. Employing the carrier conservation relation (2.45), they can be calculated as

$$\partial_{\rho_e}\big|_{\rho_e^0}\rho_h = \partial_{\rho_e}\big|_{\rho_e^0}(\rho_e + W_e - W_h) = 1 + z_e - (\partial_{\rho_e}\big|_{\rho_e^0}\rho_h)z_h$$

$$\Leftrightarrow \quad \partial_{\rho_e}\big|_{\rho_e^0}\rho_h = \frac{1+z_e}{1+z_h}, \tag{2.47a}$$

$$\partial_{\rho_e}\big|_{\rho_e^0}W_h = z_h\frac{1+z_e}{1+z_h}, \tag{2.47b}$$

where the derivative has been taken at the steady state value $\rho_e^0$ of the solitary laser. Linearizing Eqs. (2.43) around the lasing steady state $(N_{\mathrm{ph}}^0, \rho_e^0)$, yields the following characteristic equations for the growth rate $\sigma$

$$\det\begin{bmatrix} -\sigma & \frac{gR^0}{2}\left(1+\frac{1+z_e}{1+z_h}\right) \\ -\frac{\gamma 2 r_{\rm ph} R^0}{(1+z_e)g} & -\gamma\left[\begin{array}{c} r_{\rm ph}(R^0)^2\left(\frac{1}{1+z_e}+\frac{1}{1+z_h}\right) \\ +\frac{\rho_h^0}{1+z_e}+\frac{\rho_e^0}{1+z_h}+c\left(\frac{W_e^0 z_h}{1+z_h}+\frac{W_h^0 z_e}{1+z_e}\right)\end{array}\right]-\sigma \end{bmatrix} = 0, \quad (2.48)$$

where the gain-clamping $\rho^0_{\rm inv} = 0$ has been used. Solving for $\sigma$, yields two complex conjugate solutions

$$\sigma_\pm = -\gamma\Gamma_1^{\rm vf} \pm i\sqrt{\gamma r_{\rm ph}(R^0)^2\frac{c_z}{1+z_e} - \gamma^2(\Gamma_1^{\rm vf})^2} = -\gamma\Gamma_1^{\rm vf} \pm i\sqrt{\gamma}\omega_{1/2}^{\rm vf} + \mathcal{O}(\gamma^2), \quad (2.49)$$

where we have introduced

$$c_z \equiv \left(1+\frac{1+z_e}{1+z_h}\right) \quad (2.50)$$

as well as

$$\Gamma_1^{\rm vf} \equiv \frac{1}{2}\left[\frac{r_w N^0_{\rm ph}}{(1+z_e)(1+z_h)}\begin{pmatrix} 2+z_h+z_e+\rho_h^0(1+z_h)+\rho_e^0(1+z_e) \\ +c\left(W_e^0 z_h(1+z_e)+W_h^0 z_e(1+z_h)\right)\end{pmatrix}\right], \quad (2.51a)$$

$$\omega_{1/2}^{\rm vf} \equiv \sqrt{r_{\rm ph}(R^0)^2\frac{c_z}{1+z_e}} = \sqrt{r_w N^0_{\rm ph}\left(\frac{2+z_e+z_h}{(1+z_e)(1+z_h)}\right)}. \quad (2.51b)$$

Damping and frequency of the ROs are then given in terms of the dimensionless time $t'$ by

$$\Gamma^{\rm vf} \equiv \gamma\Gamma_1^{\rm vf} \quad \text{and} \quad \omega^{\rm vf} \equiv \sqrt{\gamma}\omega_{1/2}^{\rm vf}, \quad (2.52)$$

respectively. In terms of the physical time $t$, RO damping and frequency read[5]

$$\Gamma_{\rm RO}^{\rm vf} \equiv \kappa\gamma\left[\frac{(\bar{W}/W)N^0_{\rm ph}}{(1+z_e)(1+z_h)}\begin{pmatrix} 2+z_h+z_e+\rho_h^0(1+z_h)+\rho_e^0(1+z_e) \\ +\frac{B^S 2N^{\rm QD}}{W}\left(W_e^0 z_h(1+z_e)+W_h^0 z_e(1+z_h)\right)\end{pmatrix}\right], \quad (2.53a)$$

$$\omega_{\rm RO}^{\rm vf} \equiv 2\kappa\sqrt{\gamma\,(\bar{W}/W)N^0_{\rm ph}\left(\frac{2+z_e+z_h}{(1+z_e)(1+z_h)}\right)}, \quad (2.53b)$$

where $z_b$ is given as a function of the carrier densities in the reservoir $w_b$:

$$z_b = \partial_{\rho_b}\big|_{\rho_e^0} W_b = \frac{1}{2N^{\rm QD}}\partial_{\rho_b}\big|_{\rho_e^0} w_b.$$

[5] Note that $\Gamma_{\rm RO}^{\rm vf}$ and $\omega_{\rm RO}^{\rm vf}$ are given by $\Gamma_{\rm RO}^{\rm vf} = 2\kappa\gamma\Gamma_1^{\rm vf}$ and $\omega_{\rm RO}^{\rm vf} = 2\kappa\sqrt{\gamma}\omega_{1/2}^{\rm vf}$, respectively.

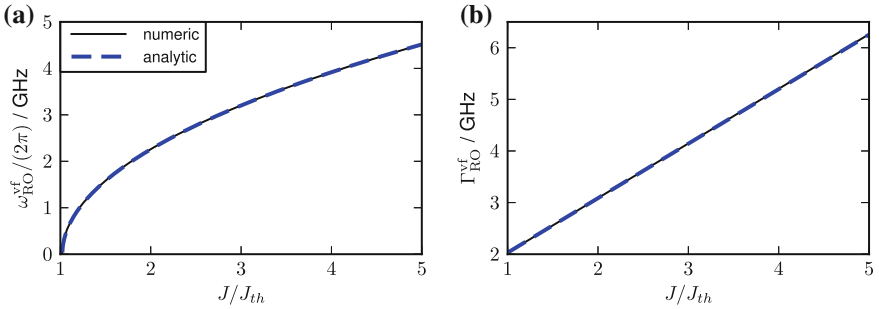


**Fig. 2.10** Comparison of RO frequency $\omega_{RO}^{S}$ (**a**) and RO damping $\Gamma_{RO}^{S}$ (**b**) as obtained numerically from the eigenvalues of the full system (*black lines*) with their analytical approximations of Eqs. (2.53) (*blue dash dotted lines*). Parameters: Very fast scattering rates and other parameters as in Table 2.3

Note that the damping scales like $\gamma$ and is thus small compared to the frequency, which scales like $\sqrt{\gamma}$. This is well known from class B semiconductor lasers [48] (see also Sect. 2.5.1). In Fig. 2.10, RO frequencies (Fig. 2.10a) and damping (Fig. 2.10b) obtained numerically from the eigenvalues of the full Eqs. (3.12) (solid black lines) are compared to the analytical approximations of Eqs. (2.53) (blue dashed lines). The analytical approximation agree perfectly with the numerical results. The square-root like increase of $\omega_{RO}^{vf}$ and the linear increase of $\Gamma_{RO}^{vf}$ with the pump current can be attributed to the linear dependence of $N_{ph}^{0}$ on the pump current (see Eq. (2.26)).

### Comparison to QW Laser

Next, the expressions for RO damping and frequency of Eqs. (2.52) are compared to the expressions obtained for the standard rate equation model for a class B laser derived in Sect. 2.5.1 (see Eqs. (2.23)). The limit of $z_e \to 0$ of Eqs. (2.52) corresponds to a decoupling of the QD levels from the carrier reservoir $\omega^{vf} \to \omega^{QW}$. If we additionally assume that both lasers have the same time scale separation ($\gamma^{QW} = \gamma$), the same ratio of the Einstein factors of spontaneous and induced emission ($r^{QW} = r_w$), and the same steady state photon number $N_{ph}^{0}$, the RO frequency of the QD laser converges to the one of the QW laser $\omega^{vf} \to \omega^{QW}$. Further, employing the limit $z_e \to 0$, we obtain for the RO damping of the QD laser $\Gamma^{vf}$ (see Eqs. (2.52))

$$\Gamma^{vf} = \frac{\gamma}{2}\left[2r_w N_{ph}^{0} + r_w N_{ph}^{0}\left(1 + \frac{1}{g}\right)\right], \quad \text{for } z_e \to 0. \tag{2.54}$$

The above expression shows that $\Gamma^{vf}$ has in the limit $z_e \to 0$ the same linear dependence on $N_{ph}^{0} \sim J - J_{th}$ and thus on the pump current $J$ as RO damping for the QW laser $\Gamma^{QW}$ (cf. Eq. (2.23a)). However, since $r_w N_{ph}^{0} > 1$ and $g > 0$,

the damping is in the limit $z_e \to 0$ larger than for the QW laser. Note however that the reduced dynamical equations (2.43) derived in the limit of very fast scattering rates are valid for strong coupling between carrier reservoir and QD levels, which is expressed by $z_e = \mathcal{O}(1)$.

## 2.6 Summary

In this chapter, a rate equation model for a QD laser has been introduced, in which the carrier exchange between discrete QD levels and the surrounding quantum well acting as a carrier reservoir is mediated by microscopically calculated Coulomb scattering rates. The latter yield carrier lifetimes $\tau_e$ and $\tau_h$ of electrons and holes in the QD levels, which depend on the band structure, i.e., on the material composition and the growth conditions of the QDs. Further, $\tau_e$ and $\tau_h$ constitute additional time scales, which are responsible for the strongly suppressed ROs of QD lasers [4, 42]. The turn-on dynamics has been discussed for three different band structures as well as in the limit of vanishing carrier lifetimes, which has revealed that band structure engineering permits to strongly influence the turn-on of the laser. Subsequently, analytical expressions for RO frequency and damping of the QD laser for different band structures have been presented and compared to the corresponding expressions for a conventional class B QW laser model. These expressions have revealed how the carrier lifetimes $\tau_e$ and $\tau_h$, i.e., the band structure, increases the turn-on damping of QD lasers if compared to the turn-on damping of QW lasers.

## References

1. D. Bimberg, M. Grundmann, N.N. Ledentsov, *Quantum Dot Heterostructures* (Wiley, New York, 1999)
2. E.U. Rafailov, M.A. Cataluna, E.A. Avrutin, *Ultrafast Lasers Based on Quantum Dot Structures* (Wiley-vch, Weinheim, 2011). ISBN: 978-3-527-40928-0
3. M. Kuntz, N.N. Ledentsov, D. Bimberg, A.R. Kovsh, V.M. Ustinov, A.E. Zhukov, YuM Shernyakov, Spectrotemporal response of 1.3 μm quantumdot lasers. Appl. Phys. Lett. **81**(20), 3846–3848 (2002)
4. T. Erneux, E.A. Viktorov, P. Mandel, Time scales and relaxation dynamics in quantum-dot lasers. Phys. Rev. A **76**, 023819 (2007). doi:10.1103/physreva.76.023819
5. K. Lüdge, E. Schöll, Quantum-dot lasers—desynchronized nonlinear dynamics of electrons and holes. IEEE J. Quantum Electron **45**(11), 1396–1403 (2009)
6. T. Erneux, E.A. Viktorov, B. Kelleher, D. Goulding, S.P. Hegarty, G. Huyet, Optically injected quantum-dot lasers. Opt. Lett. **35**(7), 070937 (2010)
7. B. Kelleher, D. Goulding, S.P. Hegarty, G. Huyet, E.A. Viktorov, T. Erneux, Chapter 1: Optically injected single-mode quantum dot lasers, in *Lecture Notes in Nanoscale Science and Technology*, ed. by Z.M. Wang (Springer, New York, 2011)
8. E. Malić, K.J. Ahn, M.J.P. Bormann, P. Hövel, E. Schöll, A. Knorr, M. Kuntz, D. Bimberg, Theory of relaxation oscillations in semiconductor quantum dot lasers. Appl. Phys. Lett. **89**, 101107 (2006). doi:10.1063/1.2346224

9. E. Malić, M.J.P. Bormann, P. Hövel, M. Kuntz, D. Bimberg, A. Knorr, E. Schöll, Coulomb damped relaxation oscillations in semiconductor quantum dot lasers. IEEE J. Sel. Top. Quantum Electron **13**(5), 1242–1248 (2007). doi:10.119/jqstqe.2007.905148
10. K. Lüdge, M.J.P. Bormann, E. Malić, P. Hövel, M. Kuntz, D. Bimberg, A. Knorr, E. Schöll, Turn-on dynamics and modulation response in semiconductor quantum dot lasers. Phys. Rev. B **78**(3), 035316 (2008). doi:10.1103/physrevb.78.035316
11. K. Lüdge, E. Schöll, Nonlinear dynamics of doped semiconductor quantum dot lasers. Eur. Phys. J. D **58**(1), 167–174 (2010)
12. K. Lüdge, Chapter 1: Nonlinear laser dynamics: From quantum dots to cryptography, in *Modeling Quantum Dot based Laser Devices*, ed. by K. Lüdge (Wiley-vch, Weinheim, 2012), pp. 3–34. ISBN: 9783527411009
13. K. Lüdge, R. Aust, G. Fiol, M. Stubenrauch, D. Arsenijevic, D. Bimberg, E. Schöll, Large signal response of semiconductor quantum-dot lasers. IEEE J. Quantum Electron **46**(12), 1755–1762 (2010). doi:10.1109/jqe.2066959.44
14. W.W. Chow, S.W. Koch, *Semiconductor-Laser Fundamentals* (Springer, Berlin, 1999). ISBN: 978-3-540-64166-7
15. Y. Su, A. Carmele, M. Richter, K. Lüdge, E. Schöll, D. Bimberg, A. Knorr, Theory of single quantum dot lasers: Pauli-blocking enhanced anti-bunching. Semicond. Sci. Technol. **26**, 014015 (2011)
16. C. Gies, J. Wiersig, M. Lorke, F. Jahnke, Semiconductor model for quantumdot- based microcavity lasers. Phys. Rev. A **75**(1), 013803 (2007)
17. D. Goulding, S.P. Hegarty, O. Rasskazov, S. Melnik, M. Hartnett, G. Greene, J.G. McInerney, D. Rachinskii, G. Huyet, Excitability in a Quantum Dot Semiconductor Laser with Optical Injection. Phys. Rev. Lett. **98**(15), 153903 (2007)
18. D. O'Brien, S.P. Hegarty, G. Huyet, A.V. Uskov, Sensitivity of quantumdot semiconductor lasers to optical feedback. Opt. Lett. **29**(10), 1072–1074 (2004)
19. G. Huyet, D. O'Brien, S.P. Hegarty, J.G. McInerney, A.V. Uskov, D. Bimberg, C. Ribbat, V.M. Ustinov, A.E. Zhukov, S.S. Mikhrin, A.R. Kovsh, J.K. White, K. Hinzer, A.J. SpringThorpe, Quantum dot semiconductor lasers with optical feedback. Phys. Stat. Sol. B **201**(2), 345–352 (2004). doi:10.1002/pssa.200303971
20. W.W. Chow, S.W. Koch, Theory of semiconductor quantum-dot laser dynamics. IEEE J. Quantum Electron **41**, 495–505 (2005). doi:10.1109/jqe.2005.843948
21. B. Lingnau, K. Lüdge, E. Schöll, W.W. Chow, Many-body and nonequilibrium effects on relaxation oscillations in a quantum-dot microcavity laser. Appl. Phys. Lett. **97**(11), 111102 (2010). doi:10.1063/1.3488004
22. B. Lingnau, K. Lüdge, E. Schöll, W.W. Chow, Dynamic many-body and nonequilibrium effects in a quantum dot microcavity laser, in *Semiconductor Lasers and Laser Dynamics IV*, ed. by K. Panajotov, M. Sciamanna, A.A. Valle, R. Michalzik. Proceedings of SPIE 49, Vol. 7720 (SPIE, Bellingham, 2010) pp.121–150. doi:10.1117/12.854671
23. B. Lingnau, K. Lüdge, W.W. Chow, E. Schöll, Influencing modulation properties of quantum-dot semiconductor lasers by electron lifetime engineering. Appl. Phys. Lett. **101**(13), 131107 (2012)
24. B. Lingnau, K. Lüdge, W.W. Chow, E. Schöll, Many-body effects and self-contained phase dynamics in an optically injected quantum-dot laser, in *Semiconductor Lasers and Laser Dynamics V, Brussels*, ed. by K. Panajotov, M. Sciamanna, A.A. Valle, R. Michalzik. Proceedings of SPIE 53, Vol. 8432 (SPIE, Bellingham, 2012), pp. 84321J–1. ISBN: 9780819491244
25. B. Lingnau, K. Lüdge, W.W. Chow, E. Schöll, Many-body effects and selfcontained phase dynamics in an optically injected quantum-dot laser, Proceedings of SPIE, Vol. 8432 (2012)
26. J. Gomis-Bresco, S. Dommers, V.V. Temnov, U. Woggon, J. Martinez-Pastor, M. Lämmlin, D. Bimberg, InGaAs quantum dots coupled to a reservoir of nonequilibrium free carriers. IEEE J. Quantum Electron **45**(9), 1121–1128 (2009)
27. M. Wegert, N. Majer, K. Lüdge, S. Dommers-Völkel, J. Gomis-Bresco, A. Knorr, U. Woggon, E. Schöll, Nonlinear gain dynamics of quantum dot optical amplifiers. Semicond. Sci. Technol. **26**, 014008 (2011). doi:10.1088/0268--1242/26/1/014008

28. N. Majer, K. Lüdge, E. Schöll, Cascading enables ultrafast gain recovery dynamics of quantum dot semiconductor optical amplifiers. Phys. Rev. B **82**, 235301 (2010)
29. N. Majer, S. Dommers-Völkel, J. Gomis-Bresco, U. Woggon, K. Lüdge, E. Schöll, Impact of carrier-carrier scattering and carrier heating on pulse train dynamics of quantum dot semiconductor optical amplifiers. Appl. Phys. Lett. **99**, 131102 (2011). doi:10.1063/1.3643048
30. N. Majer, K. Lüdge, E. Schöll, Maxwell–Bloch approach to four-wave mixing in quantum dot semiconductor optical amplifiers, in IEEE Proceeding of 11th International Conference on Numerical Simulation of Optical Devices (NUSOD), ed. by J. Piprek, (Rome, 2011) pp. 153–154. doi:10.1109/nusod.2011.6041190
31. S. Wilkinson, B. Lingnau, J. Korn, E. Schöll, K. Lüdge, Influence of noise on the signal properties of quantum-dot semiconductor optical amplifiers. IEEE J. Sel. Top. Quantum Electron **19**(4), 1900106 (2013). doi:10.1109/jstqe.2012.2233464
32. J. Pausch, C. Otto, E. Tylaite, N. Majer, E. Schöll, K. Lüdge, Optically injected quantum dot lasers - impact of nonlinear carrier lifetimes on frequency locking dynamics. New J. Phys. **14**, 053018 (2012)
33. B. Globisch, C. Otto, E. Schöll, K. Lüdge, Influence of carrier lifetimes on the dynamical behavior of quantum-dot lasers subject to optical feedback. Phys. Rev. E **86**, 046201 (2012)
34. R. Wetzler, A. Wacker, E. Schöll, Non-local Auger effect in quantum dot devices. Semicond. Sci. Technol. **19**, S43 (2004)
35. R. Wetzler, A. Wacker, E. Schöll, Coulomb scattering with remote continuum states in quantum dot devices. J. Appl. Phys. **95**, 7966 (2004)
36. M. Kuntz, Modulated InGaAs/GaAs quantum dot lasers, PhD thesis, Technische Universität Berlin, Berlin, 2006
37. M. Lorke, T.R. Nielsen, J. Seebeck, P. Gartner, F. Jahnke, Influence of carrier-carrier and carrier-phonon correlations on optical absorption and gain in quantum-dot systems. Phys. Rev. B **73**, 085324 (2006). doi:10.1103/physrevb.73.085324
38. R. Wetzler, A. Wacker, E. Schöll, C.M.A. Kapteyn, R. Heitz, D. Bimberg, Capacitance-voltage characteristics of InAs/GaAs quantum dots embedded in a pn structure. Appl. Phys. Lett. **77**, 1671 (2000)
39. A. Rack, R. Wetzler, A. Wacker, E. Schöll, Dynamical bistability in quantumdot structures: Role of auger processes. Phys. Rev. B **66**, 165429 (2002)
40. T.R. Nielsen, P. Gartner, F. Jahnke, Many-body theory of carrier capture and relaxation in semiconductor quantum-dot lasers. Phys. Rev. B **69**, 235314 (2004)
41. H.H. Nilsson, J.Z. Zhang, I. Galbraith, Homogeneous broadening in quantum dots due to Auger scattering with wetting layer carriers. Phys. Rev. B **72**(20), 205331 (2005). doi:10.1103/physrevb.72.205331
42. K. Lüdge, E. Schöll, E.A. Viktorov, T. Erneux, Analytic approach to modulation properties of quantum dot lasers. J. Appl. Phys. **109**(9), 103112 (2011). doi:10.1063/1.3587244
43. K. Lüdge E. Schöll, Temperature dependent two-state lasing in quantum dot lasers, in, Laser Dynamics and Nonlinear Photonics, Proceeding IEEE Conference Fifth Rio De La Plata Workshop, 6–9 December 2011, (IEEE Publishing Services, New York, 2012), pp. 1–6. doi:10.1109/ldnp.2011.6162081
44. E. Schöll, *Nonequilibrium Phase Transitions in Semiconductors* (Springer, Berlin, 1987)
45. H. Haken, *Laser Theory* (Springer, New York, 1983)
46. S.H. Strogatz, *Nonlinear Dynamics and Chaos* (Westview Press, Cambridge, 1994)
47. V. Flunkert, *Delay-Coupled Complex Systems* (Springer, Heidelberg, 2011). ISBN: 978-3-642-20249-0
48. T. Erneux, P. Glorieux, *Laser Dynamics* (Cambridge University Press, Cambridge, 2010)
49. S. Wieczorek, B. Krauskopf, T.B. Simpson, D. Lenstra, The dynamical complexity of optically injected semiconductor lasers. Phys. Rep. **416**(1–2), 1–128 (2005)
50. J.R. Tredicce, F.T. Arecchi, G.L. Lippi, G.P. Puccioni, Instabilities in lasers with an injected signal. J. Opt. Soc. Am. B **2**(1), 173–183 (1985). doi:10.1364/josab.2.000173
51. T. Erneux, *Applied Delay Differential Equations* (Springer, New York, 2009)

52. C. M. Bender, S. A. Orszag, Advanced Mathematical Methods for Scientists and Engineers, Vol. 1. (Springer, New York, 2010)
53. K. Lüdge, B. Lingnau, C. Otto, E. Schöll, Understanding electrical and optical modulation properties of semiconductor quantum-dot lasers in terms of their turn-on dynamics. Nonlinear Phenom. Complex Syst. **15**(4), 350–359 (2012). ISSN: 1561–4085 (Print), 1817–2458 (On)
54. J. Mørk, B. Tromborg, J. Mark, Chaos in semiconductor lasers with optical feedback-theory and experiment. IEEE J. Quantum Electron **28**, 93–108 (1992)
55. C. Otto, K. Lüdge, E.A. Viktorov, T. Erneux, Chapter 6: Quantum dot laser tolerance to optical feedback, in *Nonlinear Laser Dynamics: From Quantum Dots to Cryptography*, ed. by K. Lüdge (Wiley-vch, Weinheim, 2012), pp. 141–162. ISBN: 9783527411009
56. G.H.M. van Tartwijk, D. Lenstra, Semiconductor laser with optical injection and feedback. Quantum Semiclass. Opt. **7**, 87–143 (1995)
57. G.H.M. van Tartwijk, G.P. Agrawal, Laser instabilities: a modern perspective. Prog. Quantum Electronics **22**(2), 43–122 (1998). doi:10.1016/s0079-6727(98)00008-1
58. K. Petermann, *Laser Diode Modulation and Noise* (Kluwer Academic, Boston, 1991)
59. L.A. Coldren, S.W. Corzine, *Diode Lasers and Photonic Integrated Circuits* (John Wiley and Sons, New York, 1995)

http://www.springer.com/978-3-319-03785-1

Dynamics of Quantum Dot Lasers
Effects of Optical Feedback and External Optical Injection
Otto, C.
2014, XVII, 290 p. 92 illus., 61 illus. in color., Hardcover
ISBN: 978-3-319-03785-1